



## REVIEW

View Article Online

View Journal | View Issue

Cite this: *Inorg. Chem. Front.*, 2023, **10**, 6489

# Current progress in metal–organic frameworks and their derivatives for electrocatalytic water splitting

Yujung Chen,<sup>a</sup> Peisen Liao,<sup>\*a,b</sup> Kehan Jin,<sup>c</sup> Yun Zheng,<sup>d</sup> Huaiyu Shao <sup>d</sup> and Guangqin Li <sup>\*a</sup>

The shortage of conventional energy is a major challenge today. Electrocatalytic water splitting producing hydrogen has been widely recognized as the sustainable mode to address the energy crisis. However, its catalysts suffer from inefficiency. Metal–organic frameworks (MOFs) are a class of novel porous materials with tunable porosity and adjustable structure, which serve as valuable catalysts for electrocatalytic water splitting. Herein, the latest research progress of MOF-based materials towards efficient electrolysis of water is presented, including the design and preparation strategies of catalysts as well as the challenges faced. Firstly, the mechanism of water splitting is succinctly explicated. Subsequently, the synthesis principle and electrochemical property enhancement strategy of MOFs and their derivatives are emphatically summarized. Finally, the current major challenges of MOF-based materials are discussed, along with perspectives for future investigation directions.

Received 27th July 2023,  
Accepted 18th September 2023

DOI: 10.1039/d3qi01468a

rsc.li/frontiers-inorganic

<sup>a</sup>MOE Laboratory of Bioinorganic and Synthetic Chemistry, LIFM, IGCM, School of Chemistry, Sun Yat-sen University, Guangzhou 510006, Guangdong, China.

E-mail: liguangqin@mail.sysu.edu.cn

<sup>b</sup>School of Chemistry and Environment, Jiaying University, Meizhou 514015, Guangdong, China. E-mail: liaops3@mail.sysu.edu.cn<sup>c</sup>College of Chemistry, Macau University of Science and Technology, Macau 999078, Macau, China<sup>d</sup>Joint Key Laboratory of the Ministry of Education, Institute of Applied Physics and Materials Engineering (IAPME), University of Macau, Macau SAR, China

## 1. Introduction

In the past century, fossil fuels, including coal, oil, and gas, have been the central sources of energy for production techniques and rapid improvements in quality of life, which have caused serious greenhouse gas emissions and climate change. Refining our energy system to a sustainable and eco-friendly one is the sole approach to guarantee a habitable planet for future generations.<sup>1–5</sup> Moreover, due to the depletion of non-renewable resources, there has been significant interest in the development of renewable energy technologies.<sup>6–9</sup> In particu-



Yujung Chen

Yujung Chen received her Bachelor of Science degree from Sun Yat-sen University (China) in 2020. Currently, she is pursuing her Master's degree in Inorganic Chemistry under the supervision of Guangqin Li and focusing on the synthesis and design of metal–organic frameworks for electrochemical water splitting.



Peisen Liao

Peisen Liao received his BSc and Ph.D. degrees from Sun Yat-sen University (China) in 2015 and 2020, respectively. He went to Karlsruhe Institut für Technologie (Germany) as a visiting student from Nov. 2018 to Nov. 2019. He is currently a postdoc researcher at Sun Yat-sen University working with Prof. Guangqin Li. His research focuses on the development of novel porous nano-materials and their applications in hydrogen production and selective hydrogenation catalytic reactions.

lar, hydrogen has garnered much attention because of its high energy density, utilization ratio and eco-friendliness. Currently, the typical industrial technology for producing hydrogen includes natural gas reforming,<sup>10</sup> gasification, biomass conversion,<sup>11</sup> and electrochemical water splitting from fossil fuels, biomass, and water. Among these, electrocatalytic water splitting is a promising and sustainable solution for producing green hydrogen because it is clean, pollution-free and can be coupled with renewable energy (e.g. solar and wind power).

Electrolytic water splitting typically involves two simultaneous half-reactions: the anode produces oxygen (oxygen evolution reaction, OER), while the hydrogen evolution reaction (HER) occurs at the cathode.<sup>12,13</sup> As a promising approach to producing low-cost and high purity hydrogen gas, it has emerged as a focal point in energy-conversion technologies. Up to now, IrO<sub>2</sub>, RuO<sub>2</sub>, Pt and other precious metals are recognized as the most efficient electrocatalysts due to their unique electronic structure, leading to fast dynamics and low overpotentials.<sup>14</sup> With the development of technology, transition metal-based materials, such as layered dihydroxides (LDHs)<sup>15</sup> and metal-organic frameworks (MOFs), have been proven to be more effective than precious metals as catalysts for the OER in alkaline solutions. However, in an alkaline environment, there are scarcely any HER catalyst that exhibit catalytic efficiency surpassing that of Pt. It is urgent to develop a highly efficient and cost-effective catalyst.

MOFs, as a class of emerging porous crystalline materials, with a variety of organic ligands and metal centers are able to customize highly ordered derived carbon materials with hierarchical pores. This customization facilitates mass transfer in energy storage or conversion processes.<sup>16–20</sup> Meanwhile, their unique framework allows substance molecules from the exterior to the interior to efficiently access high-density active sites.<sup>21–23</sup>



Guangqin Li

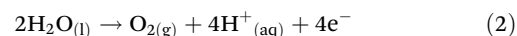
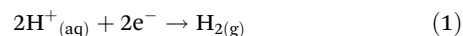
*Prof. Guangqin Li received her PhD degree from Kyoto University (Japan) under the guidance of Prof. Hiroshi Kitagawa. Then she was awarded the JSPS IKUSHI prize and worked as a JSPS Research fellow at Kyoto University. Currently, she is a full professor at the School of Chemistry at Sun Yat-sen University, China (SYSU). Her research interests focus on porous metal-organic frameworks or coordination polymer-*

*-based nanomaterials and their catalytic performance, particularly in the context of hydrogen-related applications like hydrogen production, storage and hydrogen utilization such as NO<sub>x</sub> reduction into amino acid and other organic nitrogen-containing molecules through electrocatalysis.*

Recently, MOF-based materials have been demonstrated as electrocatalysts with remarkable catalytic activity for water electrolysis. Countless researchers have devoted unremitting efforts and made great progress in this field.<sup>24,25</sup> Herein, the research progress of MOFs in electrocatalytic water splitting in recent years is summarized, and this review aims to provide a comprehensive understanding of the synthesis principles and strategies for enhancing the electrochemical properties of MOF-based materials.

## 2. Electrochemistry of water splitting

As mentioned above, electrocatalytic water splitting consists of two half-reactions:



The HER is a two-electron process as described in eqn (1),<sup>26</sup> while for the OER in eqn (2),<sup>27</sup> it is more complicated involving a four-electron process. The total reaction of electrolytic water splitting can be expressed using the following formula:



A theoretical energy difference for this reaction is  $\Delta G = 237.1 \text{ kJ mol}^{-1}$  at a thermodynamic potential of 1.23 V.<sup>28,29</sup> The detailed introduction of the HER and OER is provided below.

### 2.1 Hydrogen evolution reaction

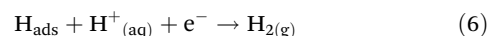
The electrochemical HER process consists of several basic steps, which are dependent on the pH of the electrolyte. Generally, the HER is more favourable under acidic conditions due to the abundance of protons present. The multi-step reaction can be summarized as a two-step reaction.<sup>30</sup> In the initial stage, hydrogen ions are absorbed on the electrode surface while electrons are provided to form adsorbed hydrogen ( $\text{H}_{\text{ads}}$ ), which is also known as the Volmer reaction (4):



$$b_{1,\text{V}} = 2.303RT/\beta F \quad (5)$$

where  $R$  represents the ideal gas constant,  $T$  represents the absolute temperature,  $F$  represents Faraday's constant, and  $\beta$  represents the symmetry factor. The first step is contingent upon the capacity for proton adsorption.

The second step is either the Heyrovsky reaction (6) or the Tafel reaction (8). If the coverage rate of  $\text{H}_{\text{ads}}$  is low and active sites are abundant on the electrode surface,  $\text{H}_{\text{ads}}$  will combine with hydrogen atoms and electrons to generate hydrogen molecule  $\text{H}_2$ .<sup>31</sup>



$$b_{1,\text{V}} = 2.303RT/(1 + \beta)F \quad (7)$$

If the coverage rate of  $H_{\text{ads}}$  is high, the two neighbouring  $H_{\text{ads}}$  will chemically combine with each other and then produce hydrogen molecules (8):



$$b_{1,v} = 2.303RT/2F \quad (9)$$

Based on the Butler–Volmer equation, the Tafel slopes  $b_{1,v}$  calculated using the above three formulas (5), (7) and (9) in different stages are  $0.118 \text{ V dec}^{-1}$ ,  $0.039 \text{ V dec}^{-1}$  and  $0.029 \text{ V dec}^{-1}$ , respectively. For example, if Tafel slope of the reaction is 0.045, the reaction mechanism is the Volmer–Heyrovsky reaction, and the reaction rate is determined by the electrochemical desorption step.

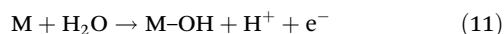
In the alkaline solution environment, the kinetics of the HER is not as fast as that in the acidic environment. The required protons for the cathode are generated through the deprotonation of hydroxide, thus affecting the kinetic process of the HER.<sup>32,33</sup> Under alkaline conditions, the cathode reactions proceed as follows (10):



## 2.2 Oxygen evolution reaction

The oxygen evolution process is much more complex involving multi-step four-electron transfer with slower reaction kinetics.<sup>34,35</sup> In an acidic or alkaline environments, different catalysts exhibit distinct kinetic processes for the OER. Noble metal catalysts (such as Ru and Ir) and their compounds have higher catalytic efficiency under acidic conditions than alkaline ones,<sup>36</sup> while transition metals such as Fe, Co and Ni have higher catalytic efficiency in alkaline environments. The M–O bond interaction has a significant effect on the stability of intermediates over the catalyst surface, and the significant difference may be a reason for the different catalytic mechanisms of the two kinds of catalysts.<sup>37,38</sup> One of the widely accepted OER mechanisms, known as the adsorbate evolution mechanism, AEM, involves the adsorption and desorption of intermediates on the metal centres, namely the  $O_{\text{Hads}} \rightarrow O_{\text{ads}} \rightarrow OOH_{\text{ads}} \rightarrow O_{2\text{ads}}$  process. The first step in all mechanisms involves the binding of hydroxide to the active site. Then the superposition of energy barriers in different steps increases the overpotential of the total reaction. The mechanisms generally agreed upon in alkalinity and acidity are as follows:

Acidic solution:



Alkaline solution:



## 2.3 Evaluation of water splitting electrocatalysts

For the purpose of comprehensively evaluating the activity of catalysts in the water splitting process, several important parameters need to be compared, including overvoltage ( $\eta$ ), Tafel slope, onset potential ( $E_{\text{onset}}$ ), exchange current density ( $j_0$ ), electrochemically active surface area (ECSA), turnover frequency (TOF) and mass or specific activity (MA or SA).<sup>16,35,39–41</sup> In the practice of electrocatalytic water splitting, the most common way to compare the activities of different electrocatalysts is to use similar loadings of active materials and compare their associated overpotentials at a given current density, such as  $10 \text{ mA cm}^{-2}$ , which has practical application values.<sup>42</sup> Beyond that, other factors such as tolerance to a wide pH range, capacity to operate at high current densities, long-term stability, the material preparation method and cost-effectiveness should also be considered.<sup>43</sup> In fact, 100% faradaic efficiency (FE) cannot be achieved by any catalyst because of the existence of different thermodynamic and kinetic barriers. As mentioned above, the best catalyst for the HER is platinum, while the best catalyst for the OER is rhodium, iridium or their compounds. However, it is impractical to use these expensive and scarce materials as catalysts, which will greatly increase the cost of electrolysis of water to produce hydrogen and is unrealistic in large-scale production. To improve the cost effectiveness and commercial viability of electrolytic water splitting, catalysts should be more efficient, affordable and stable for the OER and HER, simultaneously.

## 3. MOF-based materials for electrocatalytic water splitting

As a kind of porous catalyst for electrocatalytic water splitting, MOFs can be optimized by adjusting their chemical structure and morphology to enhance electrocatalytic performance.<sup>44</sup> The preparation methods and strategies of MOFs have been continuously developed. Simultaneously, the comprehension of MOF-based electrocatalytic water splitting has been enhanced through advancements in *in situ* spectroscopy and theoretical calculations.<sup>45</sup> Furthermore, by employing directional design for carbonized MOF materials, electrical conductivity can be significantly enhanced and more catalytic sites can be exposed, ultimately leading to improved performance in water electrolysis. In general, a significant breakthrough in the field of electrocatalytic water splitting has been achieved, and the results summarized in Table 1 show that MOFs and their derivatives offer a novel direction and concept for studying sustainable water splitting technology. The main design

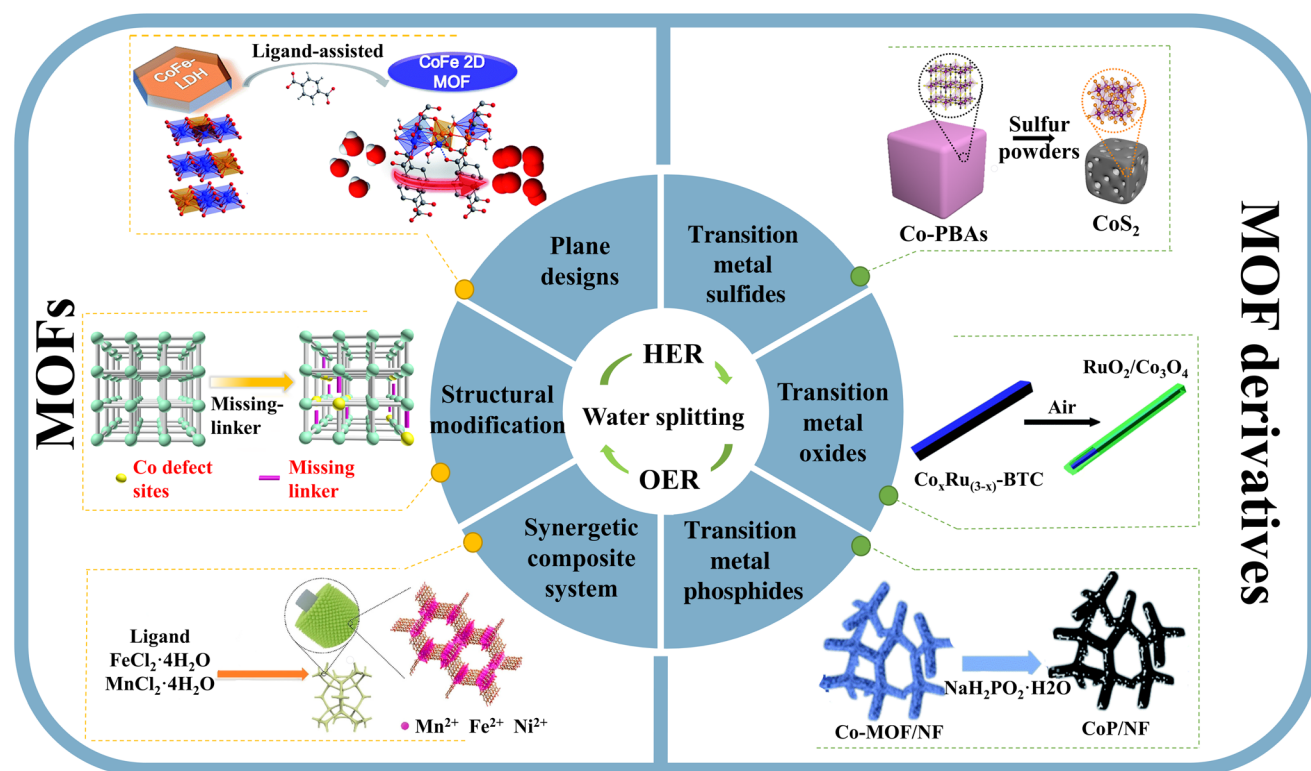
**Table 1** Overall water splitting performance of MOF-based/derived catalysts

| Catalyst  | Electrolyte                          | Overpotential (mV)         | Tafel slope (mV dec <sup>-1</sup> ) | Ref. |
|---|--------------------------------------|----------------------------|-------------------------------------|------|
| LM-160-12   | 1 M KOH                              | OER $\eta_{10}$ : 274      | 46.7                                | 60   |
| AB&CTGU-5 (1 : 4)   | 0.5 M H <sub>2</sub> SO <sub>4</sub> | HER $\eta_{10}$ : 44       | 45                                  | 61   |
| CoBDC-Fc/NF   | 1 M KOH                              | OER $\eta_{10}$ : 178      | 51                                  | 66   |
| D-Ni-MOF/NF   | 1 M KOH                              | HER $\eta_{10}$ : 101      | 50.9                                | 67   |
|   |                                      | OER $\eta_{10}$ : 219      | 48.2                                |      |
|   |                                      | OWS $\eta_{10}$ : 1.50 V   | —                                   |      |
| Ir@Ni-NDC   | 1 M KOH                              | HER $\eta_{10}$ : 19       | 28.2                                | 71   |
|   |                                      | OER $\eta_{10}$ : 210      | 44.7                                |      |
|   |                                      | OWS $\eta_{10}$ : 1.46 V   | —                                   |      |
| Ir@Ni-NDC   | 0.5 M H <sub>2</sub> SO <sub>4</sub> | HER $\eta_{10}$ : 41       | 11.1                                | 71   |
|   |                                      | OER $\eta_{10}$ : 219      | 113.0                               |      |
|   |                                      | OWS $\eta_{10}$ : 1.54 V   | —                                   |      |
| Ir@Ni-NDC   | 1 M PBS                              | HER $\eta_{10}$ : 31       | 46.9                                | 71   |
|   |                                      | OER $\eta_{10}$ : 296      | 89.3                                |      |
|   |                                      | OWS $\eta_{10}$ : 1.59 V   | —                                   |      |
| NiRu <sub>0.13</sub> -BDC   | 1 M KOH                              | HER $\eta_{10}$ : 34       | 32                                  | 72   |
|   | 1 M HCl                              | HER $\eta_{10}$ : 13       | —                                   |      |
|   | 1 M PBS                              | HER $\eta_{10}$ : 36       | 32                                  |      |
| RuCo-CAT  | 1 M KOH                              | HER $\eta_{10}$ : 38       | 32.1                                | 73   |
|   |                                      | OER $\eta_{50}$ : 315      | 45.7                                |      |
|   |                                      | OWS $\eta_{50}$ : 1.62 V   | —                                   |      |
| Mn <sub>0.52</sub> Fe <sub>0.71</sub> Ni-MOF74                          | 1 M KOH                              | HER $\eta_{100}$ : 190     | 103.8                               | 75   |
|   |                                      | OER $\eta_{100}$ : 267     | 36.7                                |      |
|   |                                      | OWS $\eta_{100}$ : 1.692 V | —                                   |      |
| CoCu-ZIF@GDY  | 1 M KOH                              | HER $\eta_{10}$ : 446      | 88                                  | 76   |
|   |                                      | OER $\eta_{10}$ : 250      | 57                                  |      |
|   |                                      | OWS $\eta_{10}$ : 1.52 V   | —                                   |      |
| Ni-MOF@Fe-MOF   | 1 M KOH                              | OER $\eta_{10}$ : 265      | 82                                  | 70   |
| Fe <sub>3</sub> O <sub>4</sub> /RuO <sub>2</sub> -C                     | 1 M KOH                              | HER $\eta_{10}$ : 94       | 68                                  | 82   |
|   |                                      | OER $\eta_{20}$ : 268      | 55                                  |      |
|   |                                      | OWS $\eta_{10}$ : 1.595 V  | —                                   |      |
| RuO <sub>2</sub> /Co <sub>3</sub> O <sub>4</sub>                        | 1 M KOH                              | HER $\eta_{10}$ : 89       | 91                                  | 83   |
|   |                                      | OER $\eta_{10}$ : 305      | 78                                  |      |
|   |                                      | OWS $\eta_{10}$ : 1.645 V  | —                                   |      |
| (Ru-Co)O <sub>x</sub>   | 1 M KOH                              | HER $\eta_{10}$ : 44.1     | 23.5                                | 84   |
|   |                                      | OER $\eta_{10}$ : 171.2    | 60.8                                |      |
|   |                                      | OWS $\eta_{10}$ : 1.488 V  | —                                   |      |
| Ni-250-2@NF   | 1 M KOH                              | HER $\eta_{10}$ : 56       | 77.43                               | 85   |
|   |                                      | OER $\eta_{10}$ : 289      | 95.63                               |      |
|   |                                      | OWS $\eta_{10}$ : 1.58 V   | —                                   |      |
| NiO/Co <sub>3</sub> O <sub>4</sub>                                      | 1 M KOH                              | HER $\eta_{10}$ : 169.5    | 119                                 | 86   |
|   |                                      | OER $\eta_{10}$ : 290      | 73                                  |      |
|   |                                      | OWS $\eta_{10}$ : 1.63 V   | —                                   |      |
| CoS <sub>2</sub> /NF  | 1 M KOH                              | HER $\eta_{10}$ : 196      | 113                                 | 88   |
|   |                                      | OER $\eta_{10}$ : 298      | 94                                  |      |
|   |                                      | OWS $\eta_{10}$ : 1.65 V   | —                                   |      |
| Co <sub>9</sub> S <sub>8</sub> @CoS@CoO@C NPs                           | 1 M KOH                              | OER $\eta_{10}$ : 28       | 81                                  | 89   |
| CoP/NF  | 1 M KOH                              | HER $\eta_{10}$ : 41.1     | 65.3                                | 91   |
|   |                                      | OER $\eta_{50}$ : 317      | 65.6                                |      |
|   |                                      | OWS $\eta_{10}$ : 1.54 V   | —                                   |      |
| CoP/NF  | 1 M PBS                              | HER $\eta_{10}$ : 55.2     | 68.7                                | 91   |
| CoP/NF  | 0.5 M H <sub>2</sub> SO <sub>4</sub> | HER $\eta_{10}$ : 83.9     | 55                                  | 91   |
| Co <sub>2</sub> P/Mo <sub>2</sub> C/Mo <sub>3</sub> Co <sub>3</sub> C@C | 1 M KOH                              | HER $\eta_{10}$ : 182      | 65                                  | 92   |
|   |                                      | OER $\eta_{10}$ : 362      | 82                                  |      |
|   |                                      | OWS $\eta_{10}$ : 1.74 V   | —                                   |      |
| FeNi <sub>2</sub> P-NPs   | 1 M KOH                              | HER $\eta_{10}$ : 170      | 70                                  | 93   |
|   |                                      | OER $\eta_{10}$ : 286      | 66                                  |      |
|   |                                      | OWS $\eta_{10}$ : 1.63 V   | —                                   |      |
| FeNiP/NCH   | 1 M KOH                              | HER $\eta_{10}$ : 216      | 125                                 | 94   |
|   |                                      | OER $\eta_{10}$ : 250      | 68                                  |      |
|   |                                      | OWS $\eta_{10}$ : 1.59 V   | —                                   |      |
| CoPO  | 1 M KOH                              | HER $\eta_{10}$ : 105      | 48                                  | 95   |
|   |                                      | OER $\eta_{10}$ : 275      | 52                                  |      |
|   |                                      | OWS $\eta_{10}$ : 1.62 V   | —                                   |      |
| Co-Zn/PNC   | 1 M KOH                              | HER $\eta_{10}$ : 180      | 100                                 | 96   |
|   |                                      | OER $\eta_{10}$ : 348      | 84                                  |      |
|   |                                      | OWS $\eta_{10}$ : 1.63 V   | —                                   |      |

Table 1 (Contd.)

| Catalyst  | Electrolyte | Overpotential (mV)        | Tafel slope (mV dec <sup>-1</sup> ) | Ref. |
|---|-------------|---------------------------|-------------------------------------|------|
| Co-Mo <sub>2</sub> N                                    | 1 M KOH     | HER $\eta_{10}$ : 76      | 47                                  | 97   |
|   |             | OER $\eta_{10}$ : 302     | 90                                  |      |
|   |             | OWS $\eta_{10}$ : 1.57 V  | —                                   |      |
| Co-NC/CF  | 1 M KOH     | HER $\eta_{10}$ : 157     | 72                                  | 98   |
|   |             | OER $\eta_{10}$ : 246     | 109                                 |      |
|   |             | OWS $\eta_{10}$ : 1.647 V | —                                   |      |
| Fe <sub>1</sub> Co <sub>2</sub> Ni <sub>1</sub> Se-MOF  | 1 M KOH     | OER $\eta_{10}$ : 260     | 54.3                                | 99   |
|   |             | HER $\eta_{10}$ : 160     | 96.2                                |      |
|   |             | OER $\eta_{10}$ : 216     | 66                                  |      |
| Fe <sub>1.2</sub> (CoNi) <sub>1.8</sub> Se <sub>6</sub> | 1 M KOH     | HER $\eta_{10}$ : 66      | 66                                  | 100  |
|   |             | OER $\eta_{10}$ : 216     | 49                                  |      |
|   |             | OWS $\eta_{10}$ : 1.55 V  | —                                   |      |

HER: hydrogen evolution reaction; OER: oxygen evolution reaction; and OWS: overall water splitting.



**Scheme 1** Illustration of the main design strategies and types of MOFs and MOF derivatives in water splitting. Reproduced with permission.<sup>60,66,75,83,88,91</sup> Copyright 2019, RSC. Copyright 2019, Springer Nature. Copyright 2020, Wiley-VCH. Copyright 2017, RSC. Copyright 2017, RSC. Copyright 2020, RSC.

strategies and types of MOFs and MOF derivatives for water splitting are illustrated in Scheme 1.

### 3.1 Intrinsic MOFs

Intrinsic MOFs, which are an emerging porous compound family,<sup>46,47</sup> exhibit scientific and technical possibilities in many fields<sup>48–51</sup> since they combine the advantages of both organic ligands and inorganic metal nodes. MOFs are highly controllable porous materials, and their electrocatalytic performance can be adjusted by designing and regulating the structure, morphology, chemical composition and composite

of MOFs with other materials. In terms of structure, physical properties such as surface area and pore size can be adjusted by manipulating the topological structure of MOFs. Meanwhile, in terms of morphology, the catalytic performance of MOFs can be influenced by the activity of the crystal face.<sup>52</sup> In terms of the chemical composition, new active sites can be introduced by adjusting the chemical structure and surface functional groups of MOFs, thus improving the catalytic performance of MOFs. In the aspect of composites, MOFs can be further improved and optimized by combining MOFs with other catalytic materials or electrode materials. In summary,



the diverse design strategies of MOF materials provide a variety of possibilities for achieving more efficient and stable MOF catalysts, exploring new avenues for perfection of the application and development of electrocatalytic water splitting.

**3.1.1 Plane design.** At the beginning of building a MOF for water splitting, the overall frame structure needs to be determined. The tortuous channels in three-dimensional MOFs can hinder the exposure and electron transport of the active sites, thus reducing the probability of contact between the active centers and reactants, leading to a decrease in catalytic activity.<sup>53,54</sup> Compared with three-dimensional (3D) MOFs, 2D MOF nanosheets have more lateral dimensions and abundant unsaturated metal active sites, which are beneficial for the combination of H<sub>2</sub>O molecules and improve electrocatalytic performance.<sup>55,56</sup> In addition, when the thickness of 2D MOF nanosheets is reduced to the nanoscale, the electrical conductivity is significantly increased, which is beneficial for their electrocatalytic performance.<sup>57</sup> 1D MOFs, possess exceptional physical and chemical properties such as a high length-diameter ratio, abundant active sites, and remarkable flexibility. Moreover, they exhibit unique geometric and electronic characteristics that facilitate the design of promising electrocatalysts. However, direct utilization of 1D MOFs as electrocatalysts is limited due to their poor conductivity and low crystallinity. Consequently, most studies involve their combination with nanoparticles or polymer nanofibers and their derivatives to enhance conductivity and stability for achieving superior performance in water splitting.<sup>58,59</sup> Besides, 2D MOF crystals with adjustable pore size, morphology and thickness can be obtained by adjusting conditions of coordination and compositions from abundant transition metal (Fe, Co, Ni, *etc.*) ions and organic ligands. For example, our group presents a novel method of converting 2D LDHs into 2D MOFs with the assistance of the ligand (Fig. 1a).<sup>60</sup> The release of the metal source from the CoFe-LDH precursor is involved in the heterogeneous nucleation process of 2D MOFs for the synthesis of CoFe bimetallic MOFs. In particular, CoFe-LDH has an adjustable and

reasonable layer spacing that facilitates ligands to attack the inner metals Co and Fe, thereby promoting the facile formation of 2D MOFs. Under alkaline conditions, the as-synthesized electrocatalyst exhibits a low overpotential of 274 mV at 10 mA cm<sup>-2</sup> and high stable activity. Furthermore, Wu *et al.* have documented the synthesis of two novel Co-MOFs, [CoL(bib)(H<sub>2</sub>O)] (CTGU-5) and [CoL(bib)]·H<sub>2</sub>O (CTGU-6) obtained in a one-pot reaction by heating a mixture of Co(ClO<sub>4</sub>)<sub>2</sub>·6H<sub>2</sub>O, naphthalene-1,4-dicarboxylic acid (L), which display distinctive coordination and lattice patterns in both 2D and 3D structures with different types of surfactant used (anionic or neutral), as illustrated in Fig. 1b.<sup>61</sup> CTGU-5 and CTGU-6 modified with glassy carbon (GC) exhibit an overpotential of 388 and 425 mV at 10 mA cm<sup>-2</sup>. Through systematic manipulation of the stoichiometric ratio between MOFs and acetylene black (AB), the optimized catalyst AB&CTGU-5 (1 : 4) exhibited the best HER performance in 0.5 M H<sub>2</sub>SO<sub>4</sub>, which can approach a current density of 10 mA cm<sup>-2</sup> with an overpotential of only 44 mV corresponding to a Tafel slope of 45 mV dec<sup>-1</sup>. The rich topological structure of MOFs can be formed by assembling distinct metal clusters such as trinuclear, octa-nuclear, and heterostructural ligands. In addition, multiple metal ions, ligand scaffolds and coordination solvent molecules can be modulated to optimize the metal center-ligand ratio, thus enabling more efficient utilization of active sites in space.<sup>62,63</sup>

**3.1.2 Structural modification.** Having determined the basic framework of the MOF building, it is necessary to refine the structure and construct different functional sites to enable them to perform their designated tasks with optimal efficiency. The electronic structure of metal centers in MOF materials can be effectively regulated and the intrinsic activity of MOF materials can be optimized through structural modification using extraneous organic ligands.<sup>64</sup> Supplementary ligands can also be used to improve the conductivity of MOF nanosheets, so as to accelerate electron transfer and improve their electrocatalytic activity.<sup>65</sup> Furthermore, the absence of the original linkers within the framework may result in the formation of defective MOFs.<sup>66</sup>

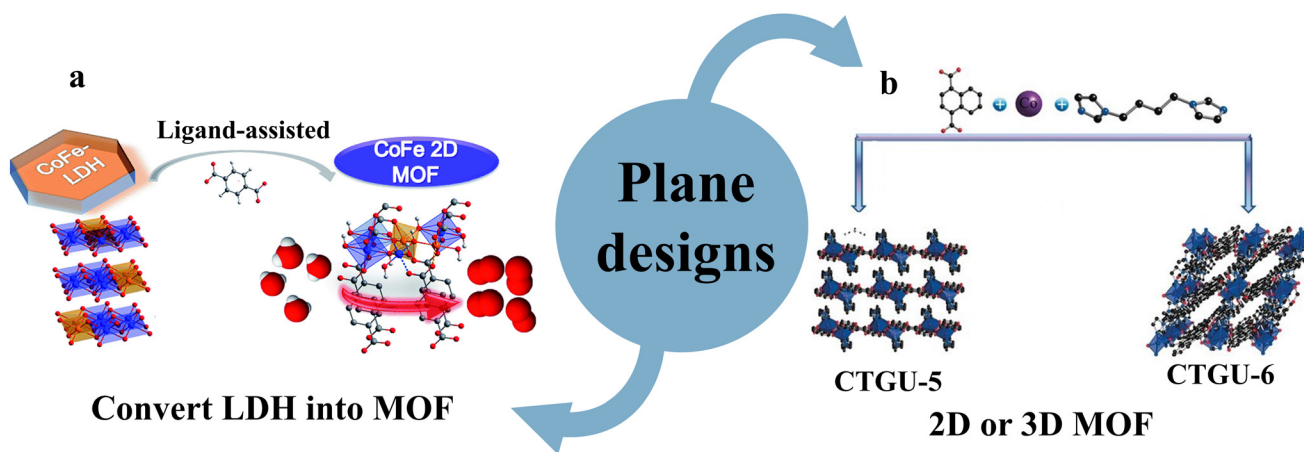


**Fig. 1** Illustration of the plane design strategies of MOF-based materials in electrocatalytic water splitting (a) convert LDH into MOF and (b) 2D or 3D MOF. Reproduced with permission<sup>60,61</sup> Copyright 2020, RSC. Copyright 2017, Wiley-VCH.

Although structural defects may cause damage to the original frame of MOFs, an appropriate degree of defects can enhance their electrochemical performance by exposing unsaturated sites and optimizing the electronic structure of active centers.

For instance, our group reported a missing-linker strategy to create unsaturated active sites, modulating the electronic structure of MOFs for improving the OER performance. In MOFs, the ligand carboxyl ferrocene (Fc) partially replaces the coordinated BDC ligand, thus changing the coordination environment of the metal center, defining the newly formed MOF as CoBDC-Fc.<sup>66</sup> The nanosheet morphology can be maintained in the process of ligand replacement. Fourier Transform Extended X-ray absorption fine structure (EXAFS) spectroscopy is used to study the local coordination of Co nodes in CoBDC and CoBDC-Fc. The coordination number of Co–O in CoBDC is 6.2, whereas that of Co–O in CoBDC-Fc is 4.4, which indicates that unsaturated Co sites are produced in CoBDC-Fc (Fig. 2a). The density functional theory (DFT) calculation shows that the binding energy between reaction intermediates and metal centers in CoBDC-Fc is optimized. CoBDC-Fc-NF requires an overpotential of only 178 mV at 10 mA cm<sup>-2</sup>, much smaller than those of CoBDC-NF (252 mV) and RuO<sub>2</sub>-NF (235 mV). Hence, the manipulation of ligands in MOFs can serve as a potent strategy for modulating the electronic structure of metal centers, thereby establishing a solid foundation for potential electrocatalytic applications.

Zhou *et al.* reported an ultra-thin array of defection-rich Ni(II)-MOF nanosheets, which was prepared by an alkali etching technique to adjust the electrocatalytic properties of overall water splitting (Fig. 2b).<sup>67</sup> Its Ni–O bonds were broken while introducing off-frame K cations in the process of alkali etching, which helps to create highly active open metal sites and greatly improves electrical conductivity. In addition, K<sup>+</sup> as conduction electrons contribute to the transfer of charge, and

increase the alkalinity of the Ni center, which can enhance the adsorption and activation of water molecules, promoting the formation of reaction intermediates, leading to high activity of overall water splitting. Therefore, the assembly of a defect-Ni-MOF||defect-Ni-MOF electrolyte cell is able to achieve a high current density water splitting reaction at a lower voltage in an alkaline medium with long-term stability.

**3.1.3 Synergetic composite system.** When the frame and structure of the MOF building have been settled, MOFs can also cooperate with other materials to construct a synergetic composite system in a well-laid-out way, optimizing the intrinsic activity of catalysts, enhancing the reaction kinetics, leading to an improvement of electrocatalytic activity.<sup>68</sup> By selectively combining MOF with other functional materials, MOF-based hybrid materials with optimized structures can be obtained, such as MOF-noble metal nanoparticles,<sup>69</sup> multi-metal collaboration, MOF-conductive substrates,<sup>70</sup> and MOF@MOFs.<sup>70</sup>

For instance, our team developed a novel electrocatalyst Ir@Ni-NDC by anchoring Ir nanoparticles on nickel-based MOF Ni-NDC (NDC: 2,6-naphthalene dicarboxylic acid).<sup>71</sup> Ir@Ni-NDC exhibits excellent electrocatalytic properties for the HER, the OER, and overall water splitting over a wide pH range due to the strong synergistic interaction between Ir and Ni-NDC *via* the Ni–O–Ir interface bond. In this work, DFT calculations show that the charge redistribution of the Ni–O–Ir bridge leads to the adsorption optimization of H<sub>2</sub>O, OH\*, and H\*, resulting in the electrochemical kinetic acceleration of the HER and OER (Fig. 3a). The Ir@Ni-NDC electrode drives 10 mA cm<sup>-2</sup> at low battery voltages in all-pH media, which is superior to the commercial Pt/C||RuO<sub>2</sub>.

Replacing noble metal nanoparticles with atomically dispersed metals can enhance atomic utilization and reduce costs. On the basis of this concept, we constructed an excellent MOF-based electrocatalyst by introducing atomically dispersed

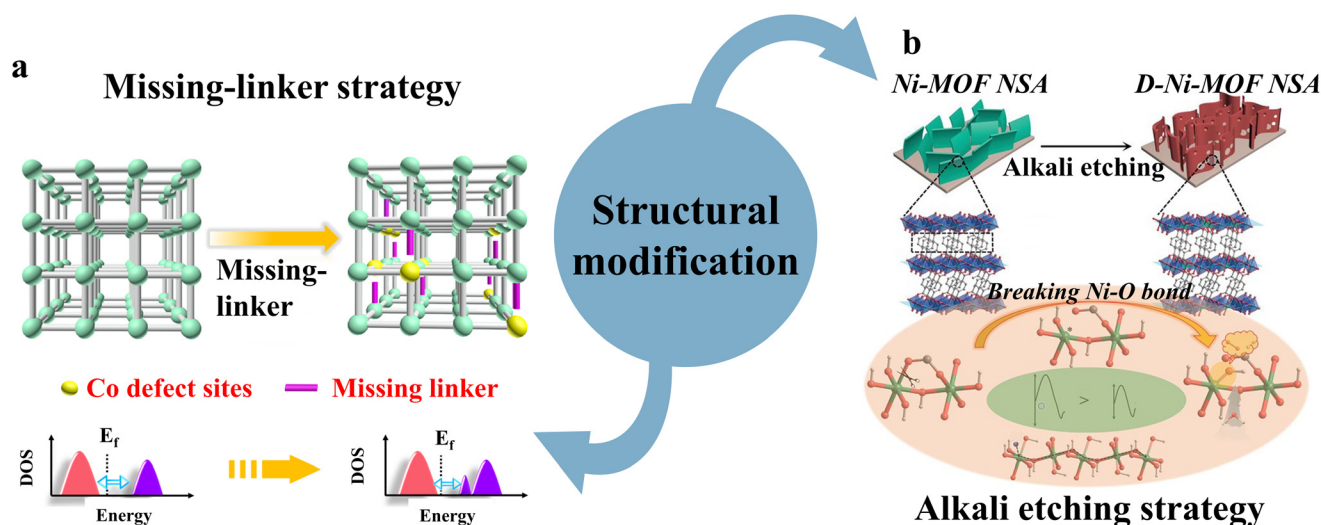
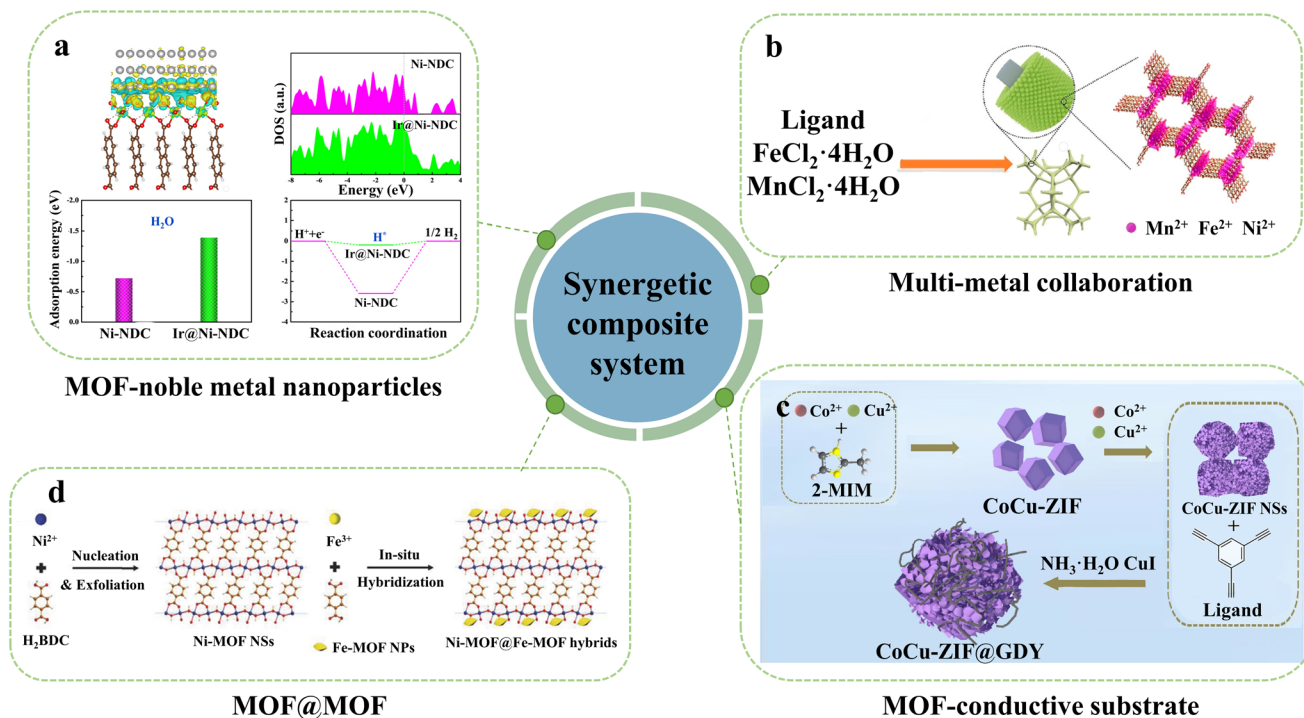


Fig. 2 Illustration of the structural modification strategies of MOF-based materials in electrocatalytic water splitting, (a) missing-linker strategy and (b) alkali etching strategy. Reproduced with permission.<sup>66,67</sup> Copyright 2020, Wiley-VCH. Copyright 2019 Springer Nature.



**Fig. 3** Illustration of the synergetic composite system of MOF-based materials in electrocatalytic water splitting, (a) MOF-noble metal nanoparticles, (b) multi-metal collaboration, (c) MOF-conductive substrate and (d) MOF@MOF. Reproduced with permission<sup>70,71,75,76</sup> Copyright 2023, Wiley-VCH. Copyright 2020, Wiley-VCH. Copyright 2020 Elsevier. Copyright 2018, Wiley-VCH.

Ru into Ni-BDC MOFs.<sup>72</sup> The optimized NiRu<sub>0.13</sub>-BDC exhibited excellent HER performance at all pH values, especially in neutral media with an overpotential as low as 36 mV at 10 mA cm<sup>-2</sup>. Through X-ray absorption fine structure (XAFS) and DFT calculations, it is shown that the introduction of a Ru single atom can adjust the electronic states of Ni in MOFs, thereby optimizing the binding strength of H<sub>2</sub>O and H\* and improving the HER performance. Chen's group also produces a double site in co-catecholate (Co-CAT) for overall water splitting by doping Ru.<sup>73</sup> The addition of a Ru atom can greatly improve the conductivity and water adsorption capacity of Co-CAT, and synergistically improve the bifunctional activity.

MOFs can also be an excellent platform for integrating multi-metal collaboration.<sup>74</sup> Our group developed a trimetallic Mn<sub>x</sub>Fe<sub>y</sub>Ni-MOF-74 film material grown *in situ* on nickel foam (Fig. 3b).<sup>75</sup> This film serves as a bifunctional electrocatalyst for overall electrocatalytic water splitting in alkaline media. The Mn<sub>0.52</sub>Fe<sub>0.71</sub>Ni-MOF-74 thin film electrode exhibits excellent performance, with overpotentials of 245 and 462 mV at 10 mA cm<sup>-2</sup> and 100 mA cm<sup>-2</sup>, respectively. The exceptional properties of the material can be attributed to the incorporation of Mn, which not only adjusts the morphology of MOF-74 to form a uniform film but also modifies the electronic structure of Fe to generate more Fe(II)-O-Fe(III) motifs, thereby promoting active site exposure and enhancing the stability of the metal site.

The catalytic capacity of MOFs can also be enhanced by assembling MOF/carbon-based functional materials. For example, Fang and colleagues have synthesized a hierarchical

electrocatalyst CoCu-ZIF@GDY with a 2D/1D nanostructure constructed using ultrathin CoCu-ZIF nanosheets with a thickness of 2 nm graphdiyne nanowires (Fig. 3c).<sup>76</sup> The composite possesses the advantages of high conductivity and exposed active sites, while its porous structure and synergistic effect between Co and Cu contribute to fast reaction kinetics. CoCu-ZIF@GDY as a bifunctional overall water-splitting catalyst has a cell voltage of 1.52 V at 10 mA cm<sup>-2</sup> in an alkaline electrolytic cell.

For the MOF@MOF synergetic composite system, Sun's group synthesized 2D Ni-MOF nanosheets modified with Fe-MOFs and demonstrated significant enhancement of catalytic activity by introducing electrochemically inert Fe-MOFs onto active Ni-MOF nanosheets (Fig. 3d).<sup>70</sup> The as synthesized Ni-MOF@Fe-MOF exhibits an overpotential of 265 mV at a current density of 10 mA cm<sup>-2</sup> in 1 M KOH. After hybridization, the overpotential experiences a reduction of approximately 100 mV owing to the distinctive morphology of 2D nanosheets and the synergistic interplay between Ni active centers and Fe.

In general, the synergistic effects of MOFs encompass the interactions among metals, ligands, and guests, which adhere to the principle of complementary advantages and collectively enhance electrocatalytic activity. During water electrolysis, several pivotal steps are involved. Initially, water molecules adsorb onto the catalyst surface and subsequently undergo cracking facilitated by the catalyst to generate an active intermediate. This intermediate then forms new molecular bonds of hydrogen and oxygen before detaching from the catalyst



surface and diffusing away. Within this catalytic cycle, different components assume distinct roles; for example, MOFs provide reaction space while accelerating material transport, incorporating conductive substrates to promote electron transport as well as introducing catalytic centers that facilitate H<sub>2</sub>O molecule cracking and the formation of hydrogen or oxygen bonds.

### 3.2 MOF derivatives

Efficient electrocatalysts can be prepared using MOFs as sacrificial templates. Under controlled temperature and atmosphere, the metal center of MOFs can be converted into oxides, phosphates, sulfides and other compounds, while organic ligands can be converted into heteroatomic-doped carbon materials. During the derivatization process, the carbonization and collapse of the MOF framework lead to the transformation of its structure into corresponding derivatives. This transformation is influenced by factors such as the initial MOF frame structure, the annealing atmosphere (*e.g.*, sulfur source, phosphorus source, nitrogen, air and argon) and the annealing procedure including the heating rate, holding temperature, annealing time and cooling rate, and they play a crucial role in determining both the graphitization degree and the derivation efficiency. Achieving high-performance derived materials necessitates the targeted design of structural composition along with precise control over annealing conditions. By manipulating the composition of precursor and applying annealing treatments, the structure of MOF derivatives can be controlled, thereby effectively enhancing their catalytic performance. Transition metal dichalcogenides (TMDCs) are innovative materials with a simple 2D structure that can rival graphene, which is typically composed of a transition metal element M (such as tungsten, molybdenum, tantalum, niobium, *etc.*) and a chalcogen element X (such as sulfur, selenium, tellurium, *etc.*) with the chemical formula MX<sub>2</sub>, known as ideal materials for optoelectronics due to their relatively low cost, ease of production into extremely thin and stable layers, and semiconductor properties.

There are many kinds of MOF derivatives, MOF precursors with special coordination environments were constructed by selecting different metals and ligands, and heteroatoms (N, S, P, O, *etc.*) were introduced into the calcination atmosphere during the derivation process involving the carbonization, oxidation or dissolution of ligands. For example, based on the electrocatalytic volcano diagram, it can be found that MoS<sub>2</sub> has excellent ability in electrolytic hydrogen evolution, and NiFeO<sub>x</sub> has efficient catalytic ability in oxygen production.<sup>77–79</sup> Therefore, in terms of collocation, we can get a rough research model for electrolytic water splitting by selecting suitable metal ions, bridging ligands and calcination atmospheres (Ar, air, H<sub>2</sub>, S, P, *etc.*), and then a more efficient catalyst can be obtained through the modification and adjustment of the MOF structure to accurately build a specific coordination environment active center for achieving water electrolysis with high-efficiency. In practical applications, catalyst cost, preparation difficulty, stability, and performance need to be taken

into consideration. As mentioned above, carbides come from a wide range of sources, oxides are easy to prepare, nitrides exhibit good electrical conductivity, and sulfides have excellent catalytic properties. Exploring how to integrate various advantages into a catalyst is what we need to focus on.

**3.2.1 Transition metal oxides.** Transition metal oxides (TMO, M = Fe, Co, Ni) with low cost, high activity and high thermodynamic stability are one of the most promising electrocatalysts in alkaline media, which was considered as the alternative to noble metals, but their low conductivity limits their further application in the field of electrocatalysis. Using MOFs as precursors, TMO loaded on conductive carbon materials can be prepared, effectively improving the conductivity of the catalyst and the dispersion of the active site. The electrochemical performance of MOF-derived oxide catalysts can be effectively improved by introducing oxygen vacancy defects<sup>80</sup> or constructing high-valence transition metal active sites.<sup>81</sup>

Coincidentally, Shekhawat *et al.* prepared an interface-rich Fe<sub>3</sub>O<sub>4</sub>/RuO<sub>2</sub>-C electrocatalyst from the MOF material,<sup>82</sup> the catalyst exhibited exceptional stability in water splitting, demonstrating an overpotential of 1.595 V at a current density of 10 mA cm<sup>-2</sup> with long-term durability. The high catalytic activity of Fe<sub>3</sub>O<sub>4</sub>/RuO<sub>2</sub>-C in alkaline media may be due to the strong synergistic interaction between Fe<sub>3</sub>O<sub>4</sub>, RuO<sub>2</sub> and C components. It is proved that Fe<sub>3</sub>O<sub>4</sub>/RuO<sub>2</sub>-C has higher catalytic activity and lower charge transfer resistance by comparing the HER, OER and Nyquist diagrams of these components. At the same time, during the heating process, Fe<sub>3</sub>O<sub>4</sub> and RuO<sub>2</sub> undergo growth while ligand carbonization, resulting in the formation of a Fe<sub>3</sub>O<sub>4</sub>/RuO<sub>2</sub>-C composite with a rich interface. The presence of both the interface and the porous structure formed after carbonization facilitates the improvement of electrocatalytic performance.

Liu and his colleagues developed a RuO<sub>2</sub>/Co<sub>3</sub>O<sub>4</sub> catalyst through annealing a cobalt-ruthenium complex derived from MOFs in an air atmosphere,<sup>83</sup> the synthetic mode is shown in Fig. 4a. Bifunctional RuO<sub>2</sub>/Co<sub>3</sub>O<sub>4</sub> was further investigated on both electrodes to evaluate its performance in overall water splitting in 1 M KOH solution, corresponding to a voltage of 1.645 V at 10 mA cm<sup>-2</sup> for the RuO<sub>2</sub>/Co<sub>3</sub>O<sub>4</sub>||RuO<sub>2</sub>/Co<sub>3</sub>O<sub>4</sub> system. Furthermore, Qi and colleagues used MOFs as templates to prepare [(Ru-Co)O<sub>x</sub>] nanosheet arrays with unique structures by *in situ* transformation.<sup>84</sup> The resulting (Ru-Co)O<sub>x</sub> catalyst showed excellent electrocatalytic activity in both the HER and the OER. The catalyst has a unique structure, optimized chemical composition, and heteroatom doping, as well as heterogeneous nanointerfaces, which contribute to its exceptional electrocatalytic activity. Specifically, the catalyst showed an overpotential of only 44.1 mV at 10 mA cm<sup>-2</sup> and a Tafel slope (23.5 mV dec<sup>-1</sup>) for the HER, and an overpotential of only 171.2 mV at 10 mA cm<sup>-2</sup> for the OER. (Ru-Co)O<sub>x</sub> also required a low cell voltage of 1.488 V at 10 mA cm<sup>-2</sup> when applied to alkaline electrolysis of water.

For Ni-based TMOs, Wang *et al.* used Ni-MOF@NF as the precursor, calcining under a mild H<sub>2</sub> atmosphere at 250 °C to

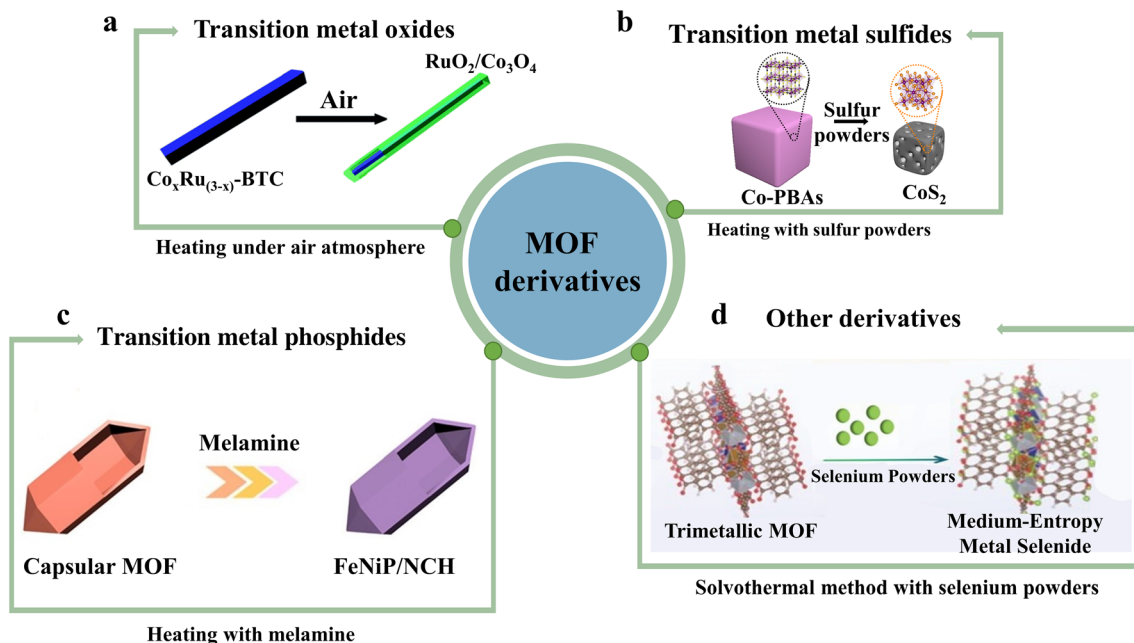


**Fig. 4** Illustration of MOF derivatives including (a) transition metal oxides, (b) transition metal sulfides, (c) transition metal phosphides and (d) other derivatives in electrocatalytic water splitting. Reproduced with permission.<sup>83,88,94,100</sup> Copyright 2017, RSC. Copyright 2019 Springer Nature. Copyright 2020, RSC. Copyright 2019, American Chemical Society.

synthesize the loose-filled nanoparticles  $\text{Ni-250-2@NF}$  structure with residual  $\text{HCOO}$  ligands.<sup>85</sup> The presence of unique organic ligands not only facilitates electron transfer, but also optimizes the hydrophilicity and oxygen phobicity of the catalyst. As a bifunctional catalyst for overall water splitting reaction,  $\text{Ni-250-2@NF}$  produces a cell voltage of 1.58 V at 10  $\text{mA cm}^{-2}$ . Mixed oxides can be formed in bimetallic MOF systems. For example, Wei *et al.* successfully developed carbon-coated  $\text{NiO/Co}_3\text{O}_4$  concave surface microcubes (NCMC) from  $\text{Ni}_3[\text{Co}(\text{CN})_6]_2$  precursors,<sup>86</sup> which showed good electrocatalytic activity and own good long cycle life for HER and OER in KOH solution, reaching 10  $\text{mA cm}^{-2}$  at 169.5 mV for HER and 290 mV for OER, respectively.

**3.2.2 Transition metal sulphides.** Recently, transition metal sulfides (TMSs) have emerged as a promising class of electrocatalysts for water splitting reactions. The strong electronegativity of sulfur atoms facilitates the regulation of electronic states in metal centers and optimizes the adsorption energy of reaction intermediates on the surface of the catalyst, resulting in good catalytic activity and fast kinetics.<sup>87</sup> MOF-derived metal sulfides can combine the conductivity of metal sulfides with the porosity of MOFs, thus synergistically promoting the electrocatalytic properties. On this basis, TMSs derived from MOFs as precursors have been widely studied in electrocatalytic hydrogen and oxygen precipitation reactions.

For instance, Joo *et al.* controlled vulcanization annealing of a cobalt Prussian blue analogue (Co-PBA) as a porous template for synthesizing  $\text{CoS}_2$  nanoparticles (Fig. 4b).<sup>88</sup> The catalytic overpotentials of the OER and the HER reached 298 and  $-196$  mV at 10  $\text{mA cm}^{-2}$ , respectively. According to the electro-

chemical characterization,  $\text{CoS}_2$  electrodes driven from Co-PBA as bifunctional electrocatalysts exhibit high electrocatalytic performance for overall water splitting due to their porous structure containing nanopores, which has been confirmed by an all-battery system. More complex  $\text{Co}_9\text{S}_8@\text{CoS}@\text{CoO}@\text{C}$  NPs were fabricated using  $\text{Co}(\text{H}_2\text{L})_2(\text{H}_2\text{O})_2 \cdot 2\text{DMF}$  ( $\text{H}_3\text{L} = 2$ -thio-barbituric acid) as precursors *via* a one-step low-temperature annealing method.<sup>89</sup> The superior synergistic effect on electrocatalytic activity at a potential of 1.38 V vs. RHE at 10  $\text{mA cm}^{-2}$  is attributed to the strong electron coupling interactions among different crystalline Co compounds and amorphous carbon, while the connection of amorphous carbon can prevent the aggregation of immobilized cobalt compounds and provide conductive channels for  $\text{OH}^-$  and active sites.

**3.2.3 Transition metal phosphides.** Transition metal phosphides (TMPs) are promising electrocatalysts with excellent electrical conductivity and metal-like properties. Phosphide-based materials are an important class of compounds with excellent electrocatalytic activity towards the HER. The phosphorylation of MOFs resulted in the formation of a carbon layer structure with uniformly dispersed phosphorylated nanoparticles. The encapsulated carbon layer not only improved the electrical conductivity of the MOF derived material, but also effectively prevented the agglomeration of phosphide particles under high currents and the reduction of catalytically active surface areas, which was beneficial for catalyst stability.

TMPs derived from MOFs are usually obtained by adding a phosphorus source during the annealing process.<sup>90</sup> For instance, Liu *et al.* have reported the production of ultrathin CoP nanosheets on nickel foam (NF) through direct phosphi-

dation of MOF-derived  $\text{Co}(\text{OH})_2$  nanosheets.<sup>91</sup> The utilization of a MOF precursor facilitates the formation of a distinctive porous ultra-thin nanosheet catalyst, characterized by the abundance of exposed active sites and boundary defects, a shortened ion diffusion path, and excellent conductivity. The obtained CoP/NF electrode demonstrates outstanding electrocatalytic performance towards the HER, exhibiting remarkable overpotentials of 41.1, 55.2, and 83.9 mV at a current density of  $10 \text{ mA cm}^{-2}$  in alkaline, neutral, and acidic solutions, respectively. Additionally, it displays small Tafel slopes of 65.3, 68.7, and 55  $\text{mV dec}^{-1}$  in the respective solutions. At the same time, the catalyst also shows good performance towards the OER. When incorporated into a two-electrode alkaline water electrolyzer, the battery requires an exceptionally low voltage of only 1.54 V to achieve a current density of  $10 \text{ mA cm}^{-2}$ .

If the MOF system is bimetallic, it is easy to obtain a variety of phosphating phases during the phosphating process. Li *et al.* reported that two kinds of bimetallic MOFs (CoMo-MOFs and NiMo-MOFs) were annealed and phosphated to synthesize two porous graphene shell coated nanoparticles ( $\text{Co}_2\text{P}/\text{Mo}_2\text{C}/\text{Mo}_3\text{Co}_3\text{C}@C$  and  $\text{Ni}/\text{Ni}_2\text{P}/\text{Mo}_2\text{C}@C$ ).<sup>92</sup> The synergy of multi-component electrochemical active sites, uniform distribution, mesoporous structure, and carbon coating facilitates charge transfer in the catalytic process under alkaline conditions.  $\text{Co}_2\text{P}/\text{Mo}_2\text{C}/\text{Mo}_3\text{Co}_3\text{C}@C$  acts as a bifunctional catalyst in the anode and cathode presenting a voltage of 1.74 V at  $10 \text{ mA cm}^{-2}$  in a self-made electrolytic cell with an alkaline electrolyte. Li *et al.* also prepared a series of Fe-Ni bimetallic phosphides with adjustable composition as efficient electrocatalysts.<sup>93</sup> By controlling the phosphating temperature, the electrocatalyst with a tubular or porous nanostructure can be selectively obtained, and the crystallinity, morphology and composition of the electrocatalysts can be well regulated. It is found that the samples with high crystallization can be obtained during the phosphating process to reduce the charge transfer resistance.

The multi-stage pores of MOFs can also be used to encapsulate the phosphorus source, and then phosphorization takes place to obtain TMPs with special configurations. Wei and colleagues have proposed a novel single-crystal capsular-MOF *via* crystal structure conversion. This open-capsule MOF exhibits high capacity for sulfur and iodine adsorption. Furthermore, the resulting capsular-MOF can be transformed into a nitrogen-doped carbon-based framework loaded with FeNi phosphide nanoparticles and numerous carbon nanotube connections through thermal cleavage-phosphorylation of melamine.<sup>94</sup> Thanks to the synergistic effect between the carbon skeleton and highly surface-exposed phosphide sites, FeNiP/NCH exhibited efficient multifunctional electrocatalytic activity of the OER and the HER achieving a low potential of 1.59 V at  $10 \text{ mA cm}^{-2}$  for overall water splitting (Fig. 4c). A MOF-derived CoPO hollow polyhedron nanostructure was conducted by Chen *et al.* by subjecting the *in situ* synthesized MOF to high-temperature annealing and Ar- $\text{N}_2$  radio frequency plasma treatment.<sup>95</sup> The MOF was then filled with P and cooled in a tubular furnace, by adjusting the flow rate of Ar- $\text{N}_2$  gas, the

Co-N bond inside the MOF was cut off, which allowed for the recombination of Co and P valence bond. The precise regulation of the P/O ratio significantly enhanced the electrocatalytic activity and stability of the catalyst. The filling of the P element also ensured the uniform distribution of catalytic active sites and effectively changed the electronic structure of the catalyst. In the test of the electrocatalytic activity for the catalyst, when the current density reaches  $10 \text{ mA cm}^{-2}$ , the overpotentials of the HER and OER are 105 and 275 mV, respectively. Additionally, the Tafel slopes were 48 and 52  $\text{mV dec}^{-1}$ , indicating the outstanding electrocatalytic activity and stability of the catalyst, making it a promising candidate for electrochemical applications.

**3.2.4 Other derivatives.** In addition to the oxides, sulfides and phosphates, other derivatives of MOFs, such as nitrides, fluorides, selenides and metal-carbon complexes, have also been applied in the field of electrocatalytic water splitting. Metal nitrides are the most common and readily available among them.

For example, Co-Zn/PNC was easily obtained through annealing and carbonizing a nitrogen-containing MOF coordination skeleton.<sup>96</sup> Shi *et al.* developed a Co-Mo<sub>2</sub>N tube based on “MOFs + MOFs” strategy. Firstly, ZIF-67 was grown on one-dimensional Mo-MOFs to form ZIF-67/Mo-MOFs by the solid-state assembly method due to the similarity of ligands, ZIF-67 derived into Co metal nanoparticles and Mo-MOF turns into Mo<sub>2</sub>N during nitriding, forming a hollow Co-Mo<sub>2</sub>N hybrid with Co outer layer on the inner core of Mo<sub>2</sub>N.<sup>97</sup> The tests indicated that the intimate effect between Co and Mo<sub>2</sub>N is beneficial for optimizing intermediate adsorption, the tubular structure of Mo<sub>2</sub>N is convenient for mass transfer, and Mo<sub>2</sub>N has good electrical conductivity, which is conducive to charge transfer, so the HER performance of the material is significantly improved. For Co-Mo<sub>2</sub>N, the overpotential of the HER is only 76 mV and when the current density is  $10 \text{ mA cm}^{-2}$ , it also has great OER activity. Therefore, Co-Mo<sub>2</sub>N can be used as both the anode and the cathode in an integrated water splitting battery with a cell voltage of 1.576 V.

It is worth mentioning that Yu, Dai, Qiu and co-workers have proposed an ultra-fast and energy-saving microwave pyrolysis method for the preparation of MOF-derived electrocatalyst Co NC/CF, which achieved significant improvements in the catalyst yield, pyrolysis time and energy consumption.<sup>98</sup> The Co-NC/CF catalyst has the optimized surface bonding ability of the reaction intermediate because the metal nanoparticles in the cobalt layer are able to form a good bond with the embedded graphite layer when electrons are rapidly transferred from the cobalt layer to the surface carbon layer. Due to this optimized structure and electron transfer process, Co-NC/CF catalysts exhibit high catalytic activity in both the HER and the OER. They found that the C atoms at the *para*- and adjacent positions of the N dopant in the graphite layer are the HER and OER active sites, respectively. Co-NC/CF exhibited excellent catalytic performance with overpotentials of only 157 and 246 mV for the HER and the OER, and its long-term stability was better than most non-precious metal electrocatalysts.

DFT calculations showed that electron transfer from Co to graphitic carbon layers occurred in Co-NC/CF, significantly enhancing the surface binding of key reaction intermediates and leading to significant catalytic activity. The two collaborative active sites for the OER or HER process have been identified, providing insight into the mechanism of the catalyst's excellent performance. The outstanding overall water splitting performance of Co-NC/CF makes it a promising candidate for practical applications in electrochemical energy conversion and storage.

In alkaline electrolytes, Zhang *et al.* reported selenoid-MOF-74 nanocomposites Fe<sub>1</sub>Co<sub>2</sub>Ni<sub>1</sub>Se-MOFs prepared by a one-step solvothermal method.<sup>99</sup> Selenization not only adjusts the MOF-74 morphology to form rod-like MOFs, but also couples selenides to MOFs. At the same time, the formation of transition metal selenides anchored on MOF-74 will promote the activity of the OER because of the excellent electron conductivity of selenides and the remodelling effect. The electrocatalyst was compared with commercial RuO<sub>2</sub> and other control samples, and the overpotential of the OER test at 10 mA cm<sup>-2</sup> was only 260 mV, indicating the effectiveness of selenization. Furthermore, Meng's group prepared Fe<sub>1.2</sub>(CoNi)<sub>1.8</sub> medium-entropy nanoparticles by selenization of MOF precursors (Fig. 4d).<sup>100</sup> The best Fe<sub>1.2</sub>(CoNi)<sub>1.8</sub>Se<sub>6</sub> showed excellent electrocatalytic properties in alkaline media. Compared with MOF precursors, the formation of medium-entropy nanoparticles increased the surface charge density and brought the D-band center closer to the Fermi level. Overall, the proposed mesentropic material strategy provides a low-cost method for manufacturing energy storage and conversion devices.

The combination of abundant MOF structures and additional nonmetallic sources yields a diverse array of metal derivatives.<sup>101,102</sup> In terms of composition, (1) carbide, the carbon-based ligands comprising the MOF framework facilitate facile formation of metal carbides, which possess high porosity and specific surface area, but it is easily oxidized at high temperatures;<sup>103,104</sup> (2) oxide. Most ligands currently employed are carboxyl groups coordinating with metals, enabling the straightforward generation of metal oxides through strong electron transfer between oxygen and metals. Therefore, metal oxides are both economical and highly active as well as thermodynamic stability, but the chemical stability is not satisfactory in the electrochemical process.<sup>105</sup> (3) In contrast, sulfides, selenides or phosphates necessitate supplementary sulfur, seleniferous or phosphorus sources during annealing to replace original oxygen coordination, rendering metal oxides more advantageous in terms of cost and safety.<sup>106</sup> However, in terms of performance, electron conduction in phosphides, selenides or sulfides is faster, and the extensive surface area and excellent conductivity offered by them provide ample sites for ion adsorption *via* electrostatic fields while facilitating high double electric layer capacitance formation, thereby favoring electrocatalytic reactions.<sup>107,108</sup> Consequently, future endeavors should focus on developing multi-component composite materials that exhibit both

superior performance and cost advantages by considering comprehensive aspects such as preparation processes and material compositions.

## 4. Conclusion and outlook

In summary, MOF-based electrocatalysts have made great progress in the field of electrocatalytic water splitting. The strategies for improving the electrocatalytic activity from plane design, structural modification, composite synergistic system and corresponding derivative materials have been introduced here. With the development of MOF materials, the emergence of new categories, such as MOF glass and MOF gels, has further enriched the MOF-based electrocatalytic system with excellent processing capability, which accelerates the industrialization process. However, there are some challenges remaining to be solved before practical applications.

The first challenge is maintaining stability. MOF-based materials encounter challenges, such as active metal centre dissolution during the electrocatalysis process, especially at high current density. Moreover, the catalyst must be adaptable to various practical environments (such as seawater electrolysis), necessitating stability in electrolytes with varying pH levels and resistance to saltwater corrosion. Therefore, expanding the applicable pH range of MOFs, and developing efficient and stable MOF catalyst materials are necessary on the way to future applications.

The second challenge is economy. Because the ultimate challenge that electrolytic water splitting faces is to enter the market, its economic feasibility must be taken into consideration. When the cost of water electrolysis for hydrogen production is lower than those of other current hydrogen production technologies, it can be popularized on a large scale. Therefore, when designing and selecting the catalyst structure, the first consideration should be the cost of the electrocatalyst, followed by the complexity of the preparation process. Although some general and scalable MOFs have been achieved for water splitting in the laboratory, industrial production requires the realization of large-scale synthesis methods with controlled morphology, precise composition, and cost-effective and environmentally friendly nature, which makes the large-scale replication of MOFs synthesized as electrode materials for industrial electrocatalytic applications still a challenge.

The final challenge is the mechanism. The electrocatalytic system is complex, and MOF-based catalysts may undergo structural changes to form hydroxyl oxides during the electrocatalytic process, which brings challenges to determine the real active sites and explore the catalytic process. The electronic and geometric structures of MOFs and their interaction with water molecules play an important role in determining their catalytic activity, and the theoretical study of MOFs and their derivatives should be deepened to understand the reaction mechanism. *In situ* tests, such as *in situ* synchrotron radiation, infrared spectroscopy, and XRD, are helpful for us to clarify the mechanism. With the continuous progress of artifi-



cial intelligence since chaptGPT is available, it may bring revolutionary breakthroughs in elucidating the catalytic mechanism process in the future.

## Author contributions

Li GQ proposed the topic of this review. Chen YR and Liao PS prepared the manuscript. Chen YR, Liao PS, Jin KH, Zheng Y, Shao HY and Li GQ collectively discussed and revised the manuscript.

## Conflicts of interest

All authors declared that there are no conflicts of interest.

## Acknowledgements

This work was supported by the Overseas High-level Talents Plan of China and Guangdong Province, the 100 Talents Plan Foundation of Sun Yat-sen University, the Program for Guangdong Introducing Innovative and Entrepreneurial Teams (2017ZT07C069), and the NSFC Projects (22075321, 21821003 and 21890380).

## References

- G. A. Deluga, J. R. Salge, L. D. Schmidt and X. E. Verykios, Renewable hydrogen from ethanol by autothermal reforming, *Science*, 2004, **303**, 993–997.
- M. Ni, D. Y. C. Leung and M. K. H. Leung, A review on reforming bio-ethanol for hydrogen production, *Int. J. Hydrogen Energy*, 2007, **32**, 3238–3247.
- M. Ni, D. Y. C. Leung, M. K. H. Leung and K. Sumathy, An overview of hydrogen production from biomass, *Fuel Process. Technol.*, 2006, **87**, 461–472.
- J. H. Xian, S. S. Li, H. Su, P. S. Liao, S. H. Wang, Y. W. Zhang, W. Q. Yang, J. Yang, Y. M. Sun, Y. L. Jia, Q. L. Liu, Q. H. Liu and G. Q. Li, Electrocatalytic synthesis of essential amino acids from nitric oxide using atomically dispersed Fe on N-doped carbon, *Angew. Chem., Int. Ed.*, 2023, **62**(26), e202304007.
- J. Xian, S. Li, H. Su, P. Liao, S. Wang, R. Xiang, Y. Zhang, Q. Liu and G. Li, Electrosynthesis of  $\alpha$ -amino acids from NO and other NO<sub>x</sub> species over CoFe alloy-decorated self-standing carbon fiber membranes, *Angew. Chem., Int. Ed.*, 2023, **62**(30), e202306726.
- S. Y. Tee, K. Y. Win, W. S. Teo, L. D. Koh, S. H. Liu, C. P. Teng and M. Y. Han, Recent progress in energy-driven water splitting, *Adv. Sci.*, 2017, **4**, 24.
- P. Ahmadi, S. H. Torabi, H. Afsaneh, Y. Sadegheih, H. Ganjehsarabi and M. Ashjaee, The effects of driving patterns and PEM fuel cell degradation on the lifecycle assessment of hydrogen fuel cell vehicles, *Int. J. Hydrogen Energy*, 2020, **45**, 3595–3608.
- J. P. Jones, G. K. S. Prakash and G. A. Olah, Electrochemical CO<sub>2</sub> reduction: recent advances and current trends, *Isr. J. Chem.*, 2014, **54**, 1451–1466.
- G. Qing, R. Ghazfar, S. T. Jackowski, F. Habibzadeh, M. M. Ashtiani, C. P. Chen, M. R. Smith and T. W. Hamann, Recent advances and challenges of electrocatalytic N<sub>2</sub> reduction to ammonia, *Chem. Rev.*, 2020, **120**, 5437–5516.
- O. Muraza and A. Galadima, A review on coke management during dry reforming of methane, *Int. J. Energy Res.*, 2015, **39**, 1196–1216.
- H. Zabed, J. N. Sahu, A. N. Boyce and G. Faruq, Fuel ethanol production from lignocellulosic biomass: An overview on feedstocks and technological approaches, *Renewable Sustainable Energy Rev.*, 2016, **66**, 751–774.
- Y. Gong, H. F. Shi, P. G. Jiang, W. Hua and J. H. Lin, Metal (II)-Induced coordination polymer based on 4-(5-(Pyridin-4-yl)-4H-1,2,4-triazol-3-yl)benzoate as an electrocatalyst for water splitting, *Cryst. Growth Des.*, 2014, **14**, 649–657.
- E. M. Miner, T. Fukushima, D. Sheberla, L. Sun, Y. Surendranath and M. Dinca, Electrochemical oxygen reduction catalysed by Ni-3(hexaiminotriphenylene)(2), *Nat. Commun.*, 2016, **7**, 7.
- X. P. Liu, M. X. Gong, S. F. Deng, T. H. Zhao, T. Shen, J. Zhang and D. L. Wang, Transforming damage into benefit: corrosion engineering enabled electrocatalysts for water splitting, *Adv. Funct. Mater.*, 2021, **31**, 29.
- X. Yu, Y. Kang, S. Wang, K. S. Hui, K. N. Hui, H. Zhao, J. Li, B. Li, J. Xu, L. Chen and H. Shao, Integrating PtNi nanoparticles on NiFe layered double hydroxide nanosheets as a bifunctional catalyst for hybrid sodium-air batteries, *J. Mater. Chem. A*, 2020, **8**, 16355–16365.
- D. Chimene, D. L. Alge and A. K. Gaharwar, Two-Dimensional nanomaterials for biomedical applications: emerging trends and future prospects, *Adv. Mater.*, 2015, **27**, 7261–7284.
- C. H. Wang, X. L. Liu, N. K. Demir, J. P. Chen and K. Li, Applications of water stable metal-organic frameworks, *Chem. Soc. Rev.*, 2016, **45**, 5107–5134.
- K. L. Zhang, H. J. Hu, L. T. Shi, B. H. Jia, H. W. Huang, X. P. Han, X. D. Sun and T. Y. Ma, Strategies for optimizing the photocatalytic water-splitting performance of metal-organic framework-based materials, *Small Sci.*, 2021, **1**, 34.
- Y. T. Qin, Z. X. Li, Y. L. Duan, J. Guo, M. T. Zhao and Z. Y. Tang, Nanostructural engineering of metal-organic frameworks: Construction strategies and catalytic applications, *Matter*, 2022, **5**, 3260–3310.
- Y. C. Yang, Y. W. Yang, Y. Y. Liu, S. L. Zhao and Z. Y. Tang, Metal-organic frameworks for electrocatalysis: beyond their derivatives, *Small Sci.*, 2021, **1**, 24.
- W. T. Koo, J. S. Jang and I. D. Kim, Metal-organic frameworks for chemiresistive sensors, *Chem*, 2019, **5**, 1938–1963.

- 22 S. Gutierrez-Tarrino, J. L. Olloqui-Sariego, J. J. Calvente, M. Palomino, G. M. Espallargas, J. L. Jorda, F. Rey and P. Ona-Burgos, Cobalt Metal-organic framework based on two dinuclear secondary building units for electrocatalytic oxygen evolution, *ACS Appl. Mater. Interfaces*, 2019, **11**, 46658–46665.
- 23 J. Guo, Y. T. Qin, Y. F. Zhu, X. F. Zhang, C. Long, M. T. Zhao and Z. Y. Tang, Metal-organic frameworks as catalytic selectivity regulators for organic transformations, *Chem. Soc. Rev.*, 2021, **50**, 5366–5396.
- 24 W. Pang, B. Shao, X. Q. Tan, C. Tang, Z. Zhang and J. Huang, Exfoliation of metal-organic frameworks into efficient single-layer metal-organic nanosheet electrocatalysts by the synergistic action of host-guest interactions and sonication, *Nanoscale*, 2020, **12**, 3623–3629.
- 25 H. Huang, Y. Zhao, Y. M. Bai, F. M. Li, Y. Zhang and Y. Chen, Conductive metal-organic frameworks with extra metallic sites as an efficient electrocatalyst for the hydrogen evolution reaction, *Adv. Sci.*, 2020, **7**, 9.
- 26 Y. M. Shi and B. Zhang, Recent advances in transition metal phosphide nanomaterials: synthesis and applications in hydrogen evolution reaction, *Chem. Soc. Rev.*, 2016, **45**, 1781–1781.
- 27 E. Fabbri, A. Habereder, K. Waltar, R. Kotz and T. J. Schmidt, Developments and perspectives of oxide-based catalysts for the oxygen evolution reaction, *Catal. Sci. Technol.*, 2014, **4**, 3800–3821.
- 28 S. Dresch, F. Dionigi, M. Klingenhof and P. Strasser, direct electrolytic splitting of seawater: opportunities and challenges, *ACS Energy Lett.*, 2019, **4**, 933–942.
- 29 J. Yu, Q. J. He, G. M. Yang, W. Zhou, Z. P. Shao and M. Ni, Recent Advances and prospective in ruthenium-based materials for electrochemical water splitting, *ACS Catal.*, 2019, **9**, 9973–10011.
- 30 D. M. Heard and A. J. J. Lennox, Electrode materials in modern organic electrochemistry, *Angew. Chem., Int. Ed.*, 2020, **59**, 18866–18884.
- 31 M. Zeng and Y. G. Li, Recent advances in heterogeneous electrocatalysts for the hydrogen evolution reaction, *J. Mater. Chem. A*, 2015, **3**, 14942–14962.
- 32 J. Zhu, L. S. Hu, P. X. Zhao, L. Y. S. Lee and K. Y. Wong, Recent advances in electrocatalytic hydrogen evolution using nanoparticles, *Chem. Rev.*, 2020, **120**, 851–918.
- 33 T. F. Jaramillo, K. P. Jorgensen, J. Bonde, J. H. Nielsen, S. Horch and I. Chorkendorff, Identification of active edge sites for electrochemical H<sub>2</sub> evolution from MoS<sub>2</sub> nanocatalysts, *Science*, 2007, **317**, 100–102.
- 34 Y. P. Chen, K. Rui, J. X. Zhu, S. X. Dou and W. P. Sun, Recent progress on nickel-based oxide/(Oxy)hydroxide electrocatalysts for the oxygen evolution reaction, *Chem. – Eur. J.*, 2019, **25**, 703–713.
- 35 N. T. Suen, S. F. Hung, Q. Quan, N. Zhang, Y. J. Xu and H. M. Chen, Electrocatalysis for the oxygen evolution reaction: recent development and future perspectives, *Chem. Soc. Rev.*, 2017, **46**, 337–365.
- 36 I. C. Man, H. Y. Su, F. Calle-Vallejo, H. A. Hansen, J. I. Martinez, N. G. Inoglu, J. Kitchin, T. F. Jaramillo, J. K. Norskov and J. Rossmeisl, Universality in oxygen evolution electrocatalysis on oxide surfaces, *ChemCatChem*, 2011, **3**, 1159–1165.
- 37 J. J. Duan, S. Chen and C. Zhao, Ultrathin metal-organic framework array for efficient electrocatalytic water splitting, *Nat. Commun.*, 2017, **8**, 7.
- 38 L. C. Seitz, C. F. Dickens, K. Nishio, Y. Hikita, J. Montoya, A. Doyle, C. Kirk, A. Vojvodic, H. Y. Hwang, J. K. Norskov and T. F. Jaramillo, A highly active and stable IrO<sub>x</sub>/SrIrO<sub>3</sub> catalyst for the oxygen evolution reaction, *Science*, 2016, **353**, 1011–1014.
- 39 Q. S. Gao, W. B. Zhang, Z. P. Shi, L. C. Yang and Y. Tang, Structural design and electronic modulation of transition-metal-carbide electrocatalysts toward efficient hydrogen evolution, *Adv. Mater.*, 2019, **31**, 35.
- 40 S. L. Jiao, X. W. Fu, S. Y. Wang and Y. Zhao, Perfecting electrocatalysts via imperfections: towards the large-scale deployment of water electrolysis technology, *Energy Environ. Sci.*, 2021, **14**, 1722–1770.
- 41 Z. P. Wu, X. F. Lu, S. Q. Zang and X. W. Lou, Non-noble-metal-based electrocatalysts toward the oxygen evolution reaction, *Adv. Funct. Mater.*, 2020, **30**, 20.
- 42 T. R. Cook, D. K. Dogutan, S. Y. Reece, Y. Surendranath, T. S. Teets and D. G. Nocera, Solar energy supply and storage for the legacy and non legacy worlds, *Chem. Rev.*, 2010, **110**, 6474–6502.
- 43 Y. Yan, B. Y. Xia, B. Zhao and X. Wang, A review on noble-metal-free bifunctional heterogeneous catalysts for overall electrochemical water splitting, *J. Mater. Chem. A*, 2016, **4**, 17587–17603.
- 44 S. L. Zhao, Y. Wang, J. C. Dong, C. T. He, H. J. Yin, P. F. An, K. Zhao, X. F. Zhang, C. Gao, L. J. Zhang, J. W. Lv, J. X. Wang, J. Q. Zhang, A. M. Khattak, N. A. Khan, Z. X. Wei, J. Zhang, S. Q. Liu, H. J. Zhao and Z. Y. Tang, Ultrathin metal-organic framework nanosheets for electrocatalytic oxygen evolution, *Nat. Energy*, 2016, **1**, 1–10.
- 45 S. L. Zhao, C. H. Tan, C. T. He, P. F. An, F. Xie, S. Jiang, Y. F. Zhu, K. H. Wu, B. W. Zhang, H. J. Li, J. Zhang, Y. Chen, S. Q. Liu, J. C. Dong and Z. Y. Tang, Structural transformation of highly active metal-organic framework electrocatalysts during the oxygen evolution reaction, *Nat. Energy*, 2020, **5**, 881–890.
- 46 H. Li, M. Eddaoudi, M. O’Keeffe and O. M. Yaghi, Design and synthesis of an exceptionally stable and highly porous metal-organic framework, *Nature*, 1999, **402**, 276–279.
- 47 S. Kitagawa and K. Uemura, Dynamic porous properties of coordination polymers inspired by hydrogen bonds, *Chem. Soc. Rev.*, 2005, **34**, 109–119.
- 48 A. G. Wong-Foy, A. J. Matzger and O. M. Yaghi, Exceptional H<sub>2</sub> saturation uptake in microporous metal-organic frameworks, *J. Am. Chem. Soc.*, 2006, **128**, 3494–3495.
- 49 R. Q. Zou, H. Sakurai and Q. Xu, Preparation, adsorption properties, and catalytic activity of 3D porous metal-

- organic frameworks composed of cubic building blocks and alkali-metal ions, *Angew. Chem., Int. Ed.*, 2006, **45**, 2542–2546.
- 50 E. Coronado, Molecular magnetism: from chemical design to spin control in molecules, materials and devices, *Nat. Rev. Mater.*, 2020, **5**, 87–104.
- 51 A. Ahmed, S. Seth, J. Purewal, A. G. Wong-Foy, M. Veenstra, A. J. Matzger and D. J. Siegel, Exceptional hydrogen storage achieved by screening nearly half a million metal-organic frameworks, *Nat. Commun.*, 2019, **10**, 1568.
- 52 J. J. Zheng, Pt-free NiCo electrocatalysts for oxygen evolution by seawater splitting, *Electrochim. Acta*, 2017, **247**, 381–391.
- 53 T. Simon-Yarza, M. Gimenez-Marques, R. Mrimi, A. Mielcarek, R. Gref, P. Horcajada, C. Serre and P. Couvreur, A Smart Metal-Organic Framework Nanomaterial for Lung Targeting, *Angew. Chem., Int. Ed.*, 2017, **56**, 15565–15569.
- 54 M. T. Zhao, Y. X. Wang, Q. L. Ma, Y. Huang, X. Zhang, J. F. Ping, Z. C. Zhang, Q. P. Lu, Y. F. Yu, H. Xu, Y. L. Zhao and H. Zhang, Ultrathin 2D metal-organic framework nanosheets, *Adv. Mater.*, 2015, **27**, 7372–7378.
- 55 W. W. Zhao, J. L. Peng, W. K. Wang, S. J. Liu, Q. Zhao and W. Huang, Ultrathin two-dimensional metal-organic framework nanosheets for functional electronic devices, *Coord. Chem. Rev.*, 2018, **377**, 44–63.
- 56 Y. Bai, G. X. Zhang, S. S. Zheng, Q. Li, H. Pang and Q. Xu, Pyridine-modulated Ni/Co bimetallic metal-organic framework nanoplates for electrocatalytic oxygen evolution, *Sci. China Mater.*, 2021, **64**, 137–148.
- 57 L. Y. Cao, Z. K. Lin, F. Peng, W. W. Wang, R. Y. Huang, C. Wang, J. W. Yan, J. Liang, Z. M. Zhang, T. Zhang, L. S. Long, J. L. Sun and W. B. Lin, Self-Supporting Metal-Organic Layers as Single-Site Solid Catalysts, *Angew. Chem., Int. Ed.*, 2016, **55**, 4962–4966.
- 58 X. Pan, Q. Zhu, K. Yu, M. Yan, W. Luo, S. C. E. Tsang and L. Mai, One-dimensional metal-organic frameworks: Synthesis, structure and application in electrocatalysis, *Next Mater.*, 2023, **1**(1), 100010.
- 59 M. M. Liu, N. Cai, V. Chan and F. Q. Yu, Development and applications of mofs derivative one-dimensional nanofibers via electrospinning: a mini-review, *Nanomaterials*, 2019, **9**, 21.
- 60 M. K. Cai, Q. L. Liu, Z. Q. Xue, Y. L. Li, Y. A. Fan, A. P. Huang, M. R. Li, M. Croft, T. A. Tyson, Z. F. Ke and G. Q. Li, Constructing 2D MOFs from 2D LDHs: a highly efficient and durable electrocatalyst for water oxidation, *J. Mater. Chem. A*, 2020, **8**, 190–195.
- 61 Y. P. Wu, W. Zhou, J. Zhao, W. W. Dong, Y. Q. Lan, D. S. Li, C. H. Sun and X. H. Bu, Surfactant-assisted phase-selective synthesis of new cobalt MOFs and their efficient electrocatalytic hydrogen evolution reaction, *Angew. Chem., Int. Ed.*, 2017, **56**, 13001–13005.
- 62 R. Z. Zhang, L. L. Lu, Z. H. Chen, X. P. Zhang, B. Y. Wu, W. Shi and P. Cheng, Bimetallic cage-based metal-organic frameworks for electrochemical hydrogen evolution reaction with enhanced activity, *Chem. – Eur. J.*, 2022, **28**, 7.
- 63 H. W. Lin, D. S. Raja, X. F. Chuah, C. T. Hsieh, Y. A. Chen and S. Y. Lu, Bi-metallic MOFs possessing hierarchical synergistic effects as high performance electrocatalysts for overall water splitting at high current densities, *Appl. Catal., B*, 2019, **258**, 12.
- 64 W. Zhou, D. D. Huang, Y. P. Wu, J. Zhao, T. Wu, J. Zhang, D. S. Li, C. H. Sun, P. Y. Feng and X. H. Bu, Stable Hierarchical bimetal-organic nanostructures as high-performance electrocatalysts for the oxygen evolution reaction, *Angew. Chem., Int. Ed.*, 2019, **58**, 4227–4231.
- 65 H. X. Jia, Y. C. Yao, J. T. Zhao, Y. Y. Gao, Z. L. Luo and P. W. Du, A novel two-dimensional nickel phthalocyanine-based metal-organic framework for highly efficient water oxidation catalysis, *J. Mater. Chem. A*, 2018, **6**, 1188–1195.
- 66 Z. Q. Xue, K. Liu, Q. L. Liu, Y. L. Li, M. R. Li, C. Y. Su, N. Ogiwara, H. Kobayashi, H. Kitagawa, M. Liu and G. Q. Li, Missing-linker metal-organic frameworks for oxygen evolution reaction, *Nat. Commun.*, 2019, **10**, 8.
- 67 J. Zhou, Y. B. Dou, X. Q. Wu, A. Zhou, L. Shu and J. R. Li, Alkali-Etched Ni(II)-based metal-organic framework nanosheet arrays for electrocatalytic overall water splitting, *Small*, 2020, **16**, 8.
- 68 W. C. Hu, Y. Shi, Y. Zhou, C. Wang, M. R. Younis, J. Pang, C. Wang and X. H. Xia, Plasmonic hot charge carriers activated Ni centres of metal-organic frameworks for the oxygen evolution reaction, *J. Mater. Chem. A*, 2019, **7**, 10601–10609.
- 69 Z. X. Xia, J. Fang, X. M. Zhang, L. P. Fan, A. J. Barlow, T. Lin, S. L. Wang, G. G. Wallace, G. Q. Sun and X. A. Wang, Pt nanoparticles embedded metal-organic framework nanosheets: A synergistic strategy towards bifunctional oxygen electrocatalysis, *Appl. Catal., B*, 2019, **245**, 389–398.
- 70 K. Rui, G. Zhao, Y. Chen, Y. Lin, Q. Zhou, J. Chen, J. Zhu, W. Sun, W. Huang and S. X. Dou, Hybrid 2D dual-metal-organic frameworks for enhanced water oxidation catalysis, *Adv. Funct. Mater.*, 2018, **28**, 9.
- 71 J. Yang, Y. Shen, Y. M. Sun, J. H. Xian, Y. J. Long and G. Q. Li, Ir nanoparticles anchored on metal-organic frameworks for efficient overall water splitting under pH-universal conditions, *Angew. Chem., Int. Ed.*, 2023, **62**(17), e202302220.
- 72 Y. M. Sun, Z. Q. Xue, Q. L. Liu, Y. L. Jia, Y. L. Li, K. Liu, Y. Y. Lin, M. Liu, G. Q. Li and C. Y. Su, Modulating electronic structure of metal-organic frameworks by introducing atomically dispersed Ru for efficient hydrogen evolution, *Nat. Commun.*, 2021, **12**, 1369.
- 73 Y. Q. He, F. Yan, X. Zhang, C. L. Zhu, Y. Y. Zhao, B. Geng, S. L. Chou, Y. Xie and Y. J. Chen, Creating dual active sites in conductive metal-organic frameworks for efficient water splitting, *Adv. Energy Mater.*, 2023, **13**, 12.
- 74 W. T. Li, X. T. Guo, P. B. Geng, M. Du, Q. L. Jing, X. D. Chen, G. X. Zhang, H. P. Li, Q. Xu, P. Braunstein and H. Pang, Rational design and general synthesis of multi-

- metallic metal-organic framework nano-octahedra for enhanced Li-S battery, *Adv. Mater.*, 2021, **33**, 9.
- 75 W. D. Zhou, Z. Q. Xue, Q. L. Liu, Y. L. Li, J. Q. Hu and G. Q. Li, Trimetallic MOF-74 films grown on ni foam as bifunctional electrocatalysts for overall water splitting, *ChemSusChem*, 2020, **13**, 5647–5653.
- 76 J. Cui, J. M. Liu, C. B. Wang, F. L. Rong, L. H. He, Y. P. Song, Z. H. Zhang and S. M. Fang, Efficient electrocatalytic water oxidation by using the hierarchical 1D/2D structural nanohybrid of CoCu-based zeolitic imidazolate framework nanosheets and graphdiyne nanowires, *Electrochim. Acta*, 2020, **334**, 11.
- 77 X. Xiao, L. J. Yang, W. P. Sun, Y. Chen, H. Yu, K. K. Li, B. H. Jia, L. Zhang and T. Y. Ma, Electrocatalytic water splitting: from harsh and mild conditions to natural seawater, *Small*, 2022, **18**, 16.
- 78 J. Li and G. F. Zheng, One-dimensional earth-abundant nanomaterials for water-splitting electrocatalysts, *Adv. Sci.*, 2017, **4**, 15.
- 79 W. Liu, H. X. Zhang, C. M. Li, X. Wang, J. Q. Liu and X. W. Zhang, Non-noble metal single-atom catalysts prepared by wet chemical method and their applications in electrochemical water splitting, *J. Energy Chem.*, 2020, **47**, 333–345.
- 80 B. H. Chen, X. B. He, F. X. Yin, H. Wang, D. J. Liu, R. X. Shi, J. N. Chen and H. W. Yin, MO-Co@N-doped carbon (M = Zn or Co): Vital roles of inactive zn and highly efficient activity toward oxygen reduction/evolution reactions for rechargeable zn-air battery, *Adv. Funct. Mater.*, 2017, **27**, 14.
- 81 W. X. Chen, Y. W. Zhang, G. L. Chen, R. Huang, Y. M. Zhou, Y. J. Wu, Y. J. Hu and K. Ostrikov, Mesoporous cobalt-iron-organic frameworks: a plasma-enhanced oxygen evolution electrocatalyst, *J. Mater. Chem. A*, 2019, **7**, 3090–3100.
- 82 A. Shekhawat, R. Samanta and S. Barman, MOF-Derived Porous Fe<sub>3</sub>O<sub>4</sub>/RuO<sub>2</sub>-C Composite for Efficient Alkaline Overall Water Splitting, *ACS Appl. Energy Mater.*, 2022, **5**, 6059–6069.
- 83 H. Z. Liu, G. L. Xia, R. R. Zhang, P. Jiang, J. T. Chen and Q. W. Chen, MOF-derived RuO<sub>2</sub>/Co<sub>3</sub>O<sub>4</sub> heterojunctions as highly efficient bifunctional electrocatalysts for HER and OER in alkaline solutions, *RSC Adv.*, 2017, **7**, 3686–3694.
- 84 C. Wang and L. Qi, Heterostructured inter-doped ruthenium-cobalt oxide hollow nanosheet arrays for highly efficient overall water splitting, *Angew. Chem., Int. Ed.*, 2020, **59**, 17219–17224.
- 85 S. M. Wang, Y. Zhang, X. Y. Deng, Z. Z. Ma, R. T. Cheng, Z. H. Wan, J. P. Li and X. G. Wang, Rational construction of loosely packed nickel nanoparticulates with residual HCOO ligands derived from a Ni-MOF for high-efficiency electrocatalytic overall water splitting, *J. Mater. Chem. A*, 2023, **11**, 5222–5232.
- 86 X. J. Wei, Y. H. Zhang, H. C. He, D. Gao, J. R. Hu, H. R. Peng, L. Peng, S. H. Xiao and P. Xiao, Carbon-incorporated NiO/Co<sub>3</sub>O<sub>4</sub> concave surface microcubes derived from a MOF precursor for overall water splitting, *Chem. Commun.*, 2019, **55**, 6515–6518.
- 87 S. Manzeli, D. Ovchinnikov, D. Pasquier, O. V. Yazyev and A. Kis, 2D transition metal dichalcogenides, *Nat. Rev. Mater.*, 2017, **2**, 15.
- 88 I. K. Ahn, W. Joo, J. H. Lee, H. G. Kim, S. Y. Lee, Y. Jung, J. Y. Kim, G. B. Lee, M. Kim and Y. C. Joo, Metal-organic framework-driven porous cobalt disulfide nanoparticles fabricated by gaseous sulfurization as bifunctional electrocatalysts for overall water splitting, *Sci. Rep.*, 2019, **9**, 10.
- 89 J. Y. Long, Y. Gong and J. H. Lin, Metal-organic framework-derived Co<sub>9</sub>S<sub>8</sub>@CoS@CoO@C nanoparticles as efficient electro- and photo-catalysts for the oxygen evolution reaction, *J. Mater. Chem. A*, 2017, **5**, 10495–10509.
- 90 G. X. Zhang, Y. L. Li, X. Xiao, Y. Shan, Y. Bai, H. G. Xue, H. Pang, Z. Q. Tian and Q. Xu, *In Situ* anchoring polymetallic phosphide nanoparticles within porous prussian blue analogue nanocages for boosting oxygen evolution catalysis, *Nano Lett.*, 2021, **21**, 3016–3025.
- 91 J. L. Liu, Y. Gao, X. X. Tang, K. Zhan, B. Zhao, B. Y. Xia and Y. Yan, Metal-organic framework-derived hierarchical ultrathin CoP nanosheets for overall water splitting, *J. Mater. Chem. A*, 2020, **8**, 19254–19261.
- 92 X. Li, X. L. Wang, J. Zhou, L. Han, C. Y. Sun, Q. Q. Wang and Z. M. Su, Ternary hybrids as efficient bifunctional electrocatalysts derived from bimetallic metal-organic frameworks for overall water splitting, *J. Mater. Chem. A*, 2018, **6**, 5789–5796.
- 93 S. M. Li, J. Y. Wang, X. Y. Lv, S. Zheng, J. Wang and Z. Q. Li, Controllable synthesis of MOFs-derived porous and tubular bimetallic Fe-Ni phosphides for efficient electrocatalytic water splitting, *Catal. Sci. Technol.*, 2023, **13**, 1512–1517.
- 94 Y. S. Wei, M. Zhang, M. Kitta, Z. Liu, S. Horike and Q. Xu, A single-crystal open-capsule metal-organic framework, *J. Am. Chem. Soc.*, 2019, **141**, 7906–7916.
- 95 W. Chen, W. Wei, K. Wang, N. Zhang, G. Chen, Y. Hu and K. Ostrikov, Plasma-engineered bifunctional cobalt-metal organic framework derivatives for high-performance complete water electrolysis, *Nanoscale*, 2021, **13**, 6201–6211.
- 96 W. C. Peng, G. X. Zheng, Y. B. Wang, S. Y. Cao, Z. Ji, Y. H. Huan, M. Q. Zou and X. Q. Yan, Zn doped ZIF67-derived porous carbon framework as efficient bifunctional electrocatalyst for water splitting, *Int. J. Hydrogen Energy*, 2019, **44**, 19782–19791.
- 97 X. Shi, A. P. Wu, H. J. Yan, L. Zhang, C. G. Tian, L. Wang and H. G. Fu, A “MOFs plus MOFs” strategy toward Co-Mo<sub>2</sub>N tubes for efficient electrocatalytic overall water splitting, *J. Mater. Chem. A*, 2018, **6**, 20100–20109.
- 98 H. Huang, S. Zhou, C. Yu, H. Huang, J. Zhao, L. Dai and J. Qiu, Rapid and energy-efficient microwave pyrolysis for high-yield production of highly-active bifunctional electrocatalysts for water splitting, *Energy Environ. Sci.*, 2020, **13**, 545–553.
- 99 X. Zhang, H. W. Pan, Y. B. Jia, Y. Zhang, Z. G. Jiang, C. J. Li, X. Li, L. H. Bao, R. G. Ma and K. Wang, Flower-



- like MOF-74 nanocomposites directed by selenylation towards high-efficient oxygen evolution, *J. Colloid Interface Sci.*, 2022, **623**, 552–560.
- 100 H. Wu, Z. C. Wang, Z. X. Li, Y. J. Ma, F. Ding, F. Q. Li, H. F. Bian, Q. X. Zhai, Y. L. Ren, Y. X. Shi, Y. R. Yang, Y. Deng, S. C. Tang and X. K. Meng, Medium-entropy metal selenides nanoparticles with optimized electronic structure as high-performance bifunctional electrocatalysts for overall water splitting, *Adv. Energy Mater.*, 2023, **13**(28), 2300837.
- 101 Q. Wang and D. Astruc, State of the art and prospects in metal-organic framework (mof)-based and mof-derived nanocatalysis, *Chem. Rev.*, 2020, **120**, 1438–1511.
- 102 C. Wang, J. Kim, J. Tang, M. Kim, H. Lim, V. Malgras, J. You, Q. Xu, J. Li and Y. Yamauchi, New strategies for novel mof-derived carbon materials based on nanoarchitectures, *Chem*, 2020, **6**, 19–40.
- 103 Z. Zheng, C. Guo, E. Wang, Z. He, T. Liang, T. Yang and X. Hou, The oxidation and thermal stability of two-dimensional transition metal carbides and/or carbonitrides (MXenes) and the improvement based on their surface state, *Inorg. Chem. Front.*, 2021, **8**, 2164–2182.
- 104 C. Zhang, Y. Ma, X. Zhang, S. Abdolhosseinzadeh, H. Sheng, W. Lan, A. Pakdel, J. Heier and F. Nüesch, Two-dimensional transition metal carbides and nitrides (mxenes): synthesis, properties, and electrochemical energy storage applications, *Energy Environ. Mater.*, 2020, **3**, 29–55.
- 105 J.-M. Kim, X. Zhang, J.-G. Zhang, A. Manthiram, Y. S. Meng and W. Xu, A review on the stability and surface modification of layered transition-metal oxide cathodes, *Mater. Today*, 2021, **46**, 155–182.
- 106 A. Indra, T. Song and U. Paik, Metal Organic Framework Derived Materials: Progress and Prospects for the Energy Conversion and Storage, *Adv. Mater.*, 2018, **30**, 25.
- 107 J. Lin, R. R. Chenna Krishna, C. Zeng, X. Lin, A. Zeb and C.-Y. Su, Metal-organic frameworks and their derivatives as electrode materials for potassium ion batteries: A review, *Coord. Chem. Rev.*, 2021, **446**, 26.
- 108 J. Wu, T. Ye, Y. Wang, P. Yang, Q. Wang, W. Kuang, X. Chen, G. Duan, L. Yu, Z. Jin, J. Qin and Y. Lei, Understanding the catalytic kinetics of polysulfide redox reactions on transition metal compounds in Li-S batteries, *ACS Nano*, 2022, **16**, 15734–15759.